CHAPTER

2

Types of ore deposits and their origin

2.1 Introduction

The crustal abundance of geochemical elements that form ore deposits containing valuable metals that can be explored for economic gain is examined in the following sections in terms of their occurrences and their respective origins, genesis and classification.

An ore is a metalliferous mineral or an aggregate of metalliferrous minerals, more or less mixed with gangue, which from the standpoint of (1) a miner, can be won at a profit, or from the standpoint of (2) a metallurgist, can be treated at a profit (Evans, 1993). On the geological point of view, mineral deposits are geochemical anomalies in the earth's crust due to their local high concentration of one or a diverse suite of trace elements [Ni, Au, Ag, Co, Cr, Sc, rare earth element (REE), platinum group elements (PGEs), high field strength elements (HFS), etc.], that may develop geochemical footprints (González-Álvarez et al., 2016). Economically, mineable aggregates of ore minerals are termed as ore bodies, ore shoots, ore deposits, or ore reserves.

There is almost every mineral at any place in or on the crust at different quantities; that is, at high, low, or trace concentrations. The minerals that occur in higher concentrations in many localities are known as abundant minerals and those in lower proportions, scarce minerals. Similarly, metals that occur in higher concentrations and lower concentrations are known as abundant and scarce metals, respectively.

Most abundant metals and minerals do not attract the attention of mineral explorers, whereas those that occur in trace amounts are of interest. Metals like gold, silver, copper, nickel, etc occur rarely in the crust, while at the same time, their uses are highly needed—just in

DOI: https://doi.org/10.1016/B978-0-12-819495-9.00002-5

accordance to the law of supply and demand: the higher the supply, the lower the demand and vice versa. Geochemical abundance and scarcity of metals when plotted using crustal abundances against production estimates allow estimates to be made of the relative rates of depletion of certain metals relatives to others (e.g., Einaudi, 2000; Laznicka, 2014; Peck and Huminicki, 2016).

Metals used in industrial and technological applications can be divided into two classes based on their abundance in the earth's crust. The geochemically abundant metals, of which there are five (Al, Fe, Mg, Mn, and Ti), constitute >0.1% by weight of the earth's crust, while the geochemically scarce metals, which embrace all other metals (including familiar ones such as Cu, Pb, Zn, Au, Ag), constitute <0.1%. In almost every rock, at least tiny amounts of all metals can be detected by sensitive chemical analysis.

2.1.1 Occurrence of ore deposits

Whether minerals can occur in higher or trace quantities (as crustal abundances, Table 2.1), there is always a level at which they can be considered economic or noneconomic. For instance, although gold is present almost everywhere in the crust, economic mineral deposits are isolated. On the other hand, although quartz is almost present everywhere in large quantities, the economic quartz needs to meet some criteria of purity, mineral associations, type, and quantity and yet, the abundance of quartz makes its price inferior to rare metals/minerals such as gold, tanzanite, etc.

It should be noted here that, average crustal values are different from upper or lower crustal values. For instance, the average Clarke value of Cu in the upper crust is 55 ppm (Ridley, 2013) but that of the average crust is about 27 ppm (Heinrich and Candela, 2014; Table 2.2). See also Hu and Gao (2008).

For an economic mineral deposit to form, four factors should be met; (1) presence of source of the ore components (metals and ligands such as S, H, C, Cl, S, or the combination), (2) transportation mechanism of the ore to an appropriate site (fluid such as H_2O, biological and/or mechanical means), (3) depositional mechanism that puts together the ore components into ore minerals, and (4) appropriate geological setting for the ore body to be preserved (e.g., Guilbert and Park, 1986).

Regarding the factors to be considered on the mineralogy of a mineral deposit so as to classify it as economic or not, Moon et al. (2006) considered the mineralogical form (e.g., native Cu vs chalcopyrite, $CuFeS_2$) and the undesirable constituents (e.g., tennantite, $Cu_{12}As_4S_{13}$ vs copper concentrates) as key factors. They summarize the information

TABLE 2.1 Relative abundances of some elements in the earth's crust.

Element	Abundance (at.%)	Abundance (wt.%)
Oxygen	63	47
Silicon	21	28
Aluminum	6.5	8
Iron	1.9	5
Calcium	1.9	3.6
Sodium	2.6	2.8
Potassium	1.4	2.6
Magnesium	1.8	2.1
Titanium		0.44
Hydrogen		0.14
Manganese		0.1
Phosphorus		0.1
Cu, Cr, Ni, Pb, Zn,		10^{-2}–10^{-3} each
Mn, Sn, U, W		$\sim 10^{-4}$ each
Ag, Hg		$\sim 10^{-6}$ each
Au, Pt		$\sim 10^{-7}$ each

Bailey, R.A., Clark, H.M., Ferris, J.P., Krause, S., Strong, R.L., 2002. The earth's crust. In: Ronald A. Beiley, (ed), Chemistry of the Environment, second edition, pp. 443–482, Academic Press, 835p.

that is required from a sample in order to know whether a given deposit is economic or not includes some, or all, of the following: (1) grade of the economic minerals, (2) the bulk chemical composition, (3) the minerals present, (4) the proportions of each of these minerals and their chemical compositions, (5) their grain size, (6) their textures and mineral locking patterns, and (7) any changes in these features from one part of an ore body to another.

Of the items (1)–(7) listed previously, item (4) on mineral proportions is briefly explained as an example of information useful in determining whether an ore body is economic or not. Consider mineralized systems of PGEs. Strong correlations between Pt/Ti, Pd/Ti, and Rh/Ti ratios indicate mineralized systems of PGE as compared to other variations attributable to magmatic processes, such as olivine accumulation and fractionations that can be depicted from variations of PGE/Ti ratios (Fiorentini et al., 2018). An unusual high concentration of SiO_2, MgO, and Cr and low Al_2O_3 comprise 75% of the world PGE resource,

TABLE 2.2 Typical mineable ore cutoff grades of selected elements in comparison with their average crustal abundance.

Element	Deposit type	Typical ore grade (ppm = gt^{-1})	Concentration in crust (ppm)	Enrichment factor	Largest deposits (example)	Tonnage	Grade
Al	Lateritic bauxite	240,000	84,200	3	Weipa (Australia)	149 Mt	28%
Fe	Banded iron formation upgraded	640,000	52,200	12	Mount whaleback (Australia)	>1800 Mt	65.0%
Ti	Mafic intrusions (ilmenite)	80,000	57,000	14	Lac tio (Canada)		
P	Marine sedimentary deposits	100,000	570	180	Meade Peak member (United States)	$>10^{11}$ Mt	10%
V	Layered mafic intrusions (magnetite)	2000	138	14	Bushveld Complex (South Africa)	50 Mt	0.8%
Cr	Layered mafic intrusions (chromite)	160,000	135	1200	Bushveld Complex (South Africa)	2700 Mt	19%
Zn	Stratiform Pb–Zn–Ag deposits	87,000	72	1200	Broken Hill (Australia)	284 Mt	11%
Ni	Magnetic Ni–Cu–Sulfide	13,000	59	220	Jinchuan, Baijiazuizi (China)	515 Mt	1.1%
Rb	Pegmatites from Rb-bearing Lepidolite	5000	49	100	Tanco (Canada)	0.5 Mt	1.0%
Cu		5000	27	180	El Taniente (Chile)	2850 Mt	1.3%
Cu	Hosted deposited copper sediments	23,000	27	850	Lubin (Poland)	2600 Mt	2.0%
Pb	Stratiform Pb–Zn–Ag deposits	47,000	11	4300	Broken Hill (Australia)	160 Mt	2.0%

Nb	Carbonitites	1900	8	240	Seis Lagos (Brazil)	2898 t	2%
Eu	Carbonitites	1300	1.1	1200	Bayan obo (China)	750 Mt	4.1%
W	Skarn replacement, and vein deposits	3300	1	3300	Shizhuayan (Skarn, China)	270 Mt	0.22%
Mo	Porphryry molybdenum deposits	2000	0.8	2500	Climax (Colorado, United States)	769 Mt	0.22%
Ta	Pegmatites	1800	0.7	2600	Tanco (Canada)	2.07 Mt	0.18%
Ag	Polymetallic vein deposits	160	0.056	2900	Cerro Rico de Potosi (Bolivia)	985 Mt	166 gt^{-1}
In	Volcanic-hosted massive sulfide deposits	24	0.052	500	Kidd Creek (Canada)	134 Mt	50 gt^{-1}
Hg	Epithermal veins and breccias	10,000	0.030	300,000	Almaden (Spain)	40 Mt	>1%
Pt	Magmatic PGE–Ni–Cu sulfide deposits	3	0.0015	2000	Bushveld Complex (South Africa)	9815 Mt	2.3 gt^{-1}
Au	Hydrothermal vein deposits	2	0.0013	1200	Muruntau (Uzbekistan)	2200 Mt	2.4 gt^{-1}
Au	Modified Archean placers	5	0.0013	4000	Witwatersrand Basin (South Africa)	$>10^4$ Mt	5 gt^{-1}

PGE, Platinum group element.

Tonnage (total mass of mined and economically mineable ore) and average grade of some of the largest ore deposits of each type. All values in weights units. Average concentration in crust from Rudnick and Gao (2003). Estimates of average grades indicative only, mostly based on USGS and Canadian Geological Survey compilations but partly representing single big deposits. Grades and tonnages of some of the largest deposits mostly represent single mines, but in the case of the Meade Peak phosphorite, the Bushveld Complex, and the Witwaters and Basin are estimates for one or several rock units that are mineralized at presently economic ore grades for the respective elements (Heinrich and Candela, 2014).

From Heinrich, C.A., Candela, P.A., 2014. Fluids and ore formation in the Earth's crust. In: Treatise on Geochemistry, pp. 1–28.

Bushveld complex, Great Dyke of Zimbabwe, and Still Water (Naldrett, 2010). The Fe oxide–Cu–Au (IOCG) deposits are commonly associated with presulfide sodic or sodic–calcic alteration and have abundant to low Ti–Fe oxides and/or Fe silicates intimately associated with, but generally paragenetically older than, Fe–Cu sulfides, have light rare earth elements (LREE) enrichment and low S-sulfides [lack of abundant pyrite (Groves et al., 2010)]. According to Macheyeki (2011), Pd/V and (Pd/V)/(Cu/Cr) ratios discriminate between barren and mineralized environments (see Chapter 3: Conventional and nonconventional exploration techniques—principles,and Chapter 4: Application of nonconventional mineral exploration techniques—case studies for details).

2.1.2 Genesis and classification of ore deposits

2.1.2.1 Syngenetic and epigenetic genesis of ore deposits

Ore deposits of economic value are formed under varied geological conditions. Two groups of ore deposits may be established syngenetic and epigenetic depending on their formation time relationship to the rocks associated with them (Robb, 2005). Syngenetic mineral deposits are formed at the same time as the associated rocks as in magmatic segregation during the orthomagmatic stage of consolidation of magma or during precipitation of sedimentary rocks. Formation of ore deposits in gossans and laterites due to in situ residual gossans are also considered as syngenetic because as the new rock (laterite, bauxite, kaolinite, or duricrust) is formed it is at that same time the ore deposit is formed.

The epigenetic mineral deposits are formed later after the enclosing or host rocks have been formed in filled or opened fissures in the country rocks and such ore bodies are called lodes or veins. These vein and lode deposits occur as in interstices of the country where the rock forms first and then ores form as impregnations or replacements of the country rock. In contact metamorphism mineral deposits form irregular ore bodies on the margins of metamorphosed rocks. In sedimentary rocks epigenetic processes, ore deposits are formed due to weathering and deposition of detrital sedimentary rocks in basins where placer deposits are emplaced.

2.1.2.2 Origin and classification

Ore deposits can be classified according to the genesis of the deposits (e.g., Cox and Singer, 1986), host rocks such as shale hosted deposits (Misra, 2000; Robb, 2005; Moon et al., 2006), breccia pipes, the minerals contained within the deposit such as porphyry copper deposits (e.g.,

Moon et al., 2006), and the shape or size of the deposit such as strataform and stratabound deposits (Evans and Moon, 2006).

Basic genetic processes that lead to the concentration of minerals include (1) magmatic mineral deposits that get concentrated in igneous rocks; (2) hydrothermal mineral deposits that form in association with magma and water; (3) sedimentary mineral deposits that are precipitated from a solution, typically seawater; (4) placer minerals sorted and distributed by flow of water (or ice); and (5) residual mineral deposits formed by weathering reactions at the earth's surface (e.g., Moon et al., 2006). Meyer (1981) ore classification is based on both genetic type and rock association. The classification based on both genesis and rock association relates the rock-forming process to ore-forming process, which is more descriptive empirical observation as compared to the genetic linkage alone that tends to have controversy (e.g., Robb, 2005).

Major theories of ore genesis are diverse (Niggli, 1929; Schneider, 1964; Lindgren, 1922, 1933; Bateman, 1950; Guilbert and Park, 1986; Stanton, 1972); in other words, there are no acceptable theories that can explain the entire ore genesis we see today. Stanton (1972) in his account gives much detail on these theories and the reader is referred to that work and the references therein for details. The reader should be cautioned, however, that very often several processes contribute to the formation of an ore body. Thus where we have rising hot aqueous solution forming an epigenetic stockwork deposit just below the surface and passing on upward through it to form a contiguous syngenetic deposit under, say, marine condition, even the above simple classification is facing difficulties. This is the reason why ore geologists, besides producing a plethora of ore genesis theories, have also created a plethora of ore body classification! (e.g., Ridley, 2013).

While in the 19th century, classifications of ore deposits were based on form, texture, and mineral content, Niggli's classification in 1929 was based on volcanic–plutonic rocks and that of Lindgren's classification in 1933 was based on depth temperature. Schneider's classification (1941) was based related to magmatic processes, the latter 20th century to-date classification emphasizes on theories of genesis and environment of deposition (transport medium). In the latter classification, types of ore deposits are presented along with their nature of forming processes.

There are basically three types of ore deposits based on their environment of deposition and genesis: (1) deposits due to internal processes, (2) deposits due to external/surface processes, and (3) deposits due to both internal and surface processes (after Moon, 2016). However, based on ore genetic origin, there are two types of ore deposits: (1) ore deposits formed out of or related to igneous intrusions, such as porphyry-type deposits (PD) and IOCG and (2) sedimentary deposits such as

Carlin-type and Mississippi Valley type (MVT) deposits (Cline et al., 2005; Leach et al., 2005; Seedorff et al., 2005; Williams et al., 2005; Groves et al., 2010; Richards, 2011; Vigneresse, 2019). In this book, classification based on genetic and environment of formation/deposition has been adopted.

2.1.2.3 *Deposits due to internal processes*

Deposits in this group include magmatic (orthomagmatic) ore deposits (Robb, 2005; Moon et al., 2006; Heinrich and Candela, 2014; Moon, 2016). These deposits form as a result of element enrichment from melts at high temperature without essential involvement of aqueous fluids (Heinrich and Candela, 2014). In this type of deposits, heat source (engine) is required in order to drive magmas from different sources in the form of convective cells at a global scale taking fertile magma in the mantle to the crust (e.g., Robb, 2005; Heinrich and Candela, 2014). By so doing, one or several magmatic melt phases are involved that would lead to element partitioning between melts and a phase to be favored is enriched with elements that form the ore deposit (e.g., Robb, 2005; Moon et al., 2006; Heinrich and Candela, 2014). An obvious question would be why some parts of the mantle magma are "fertile?" Some magmas can be more fertile than the other because either those magmas inherited surplus of potential ore-forming trace elements or because their source was already enriched in those components (Robb, 2005). Orthomagmatic deposits can be subdivided into:

1. Deposits formed by crystallization of magma (during differentiation of a silicate melt). Chromium, a lithophile element, is a good example of a mineral that crystallizes from silicate magma as a result of magmatic differentiation (e.g., Ridley, 2013). Chromium is a compatible mineral in spinel and in clinopyroxene crystals relative to ultramafic and mafic melts. Further, chromium can largely be retained in the mantle during partial melting and occurs in significantly lower concentrations in average crust ($\sim$100 ppm) than in mantle (concentrations up to 1%).

   Highest concentration of Cr in the crust occurs within ultramafic layers of large mafic–ultramafic igneous bodies and chromites in ultramafic rocks are solid solutions with varying amounts of Al^{3+} and Fe^{3+} replacing Cr^{3+}, and Mg^{2+} replacing Fe^{2+} (Ridley, 2013). Chromite ores are bodies with greater than about 30% chromite, in many cases almost monomineralic chromitite (=chromite rock), in mafic and ultramafic intrusive rocks. Two common types of chromite deposits are recognized on the basis of ore body form and their geological environment: stratiform chromite deposits in large, layered ultramafic–mafic intrusions; and podiform chromite ores in

ophiolites or "Alpine peridotites" (Ridley, 2013). Examples of these types of deposits are the Cr deposits in the Bushveld complex in the Republic of South Africa and the Cr in the Great Dyke of Zimbabwe. Also magma crystallized deposits are exemplified by the V-magnetite, Ilmenite in mafic intrusions (Heinrich and Candela, 2014).

Segregation of sulfide melt from silicate melt (i.e., formation of immiscible sulfide melt phases)—the processes that lead to the formation of Ni−Cu sulfide deposits in mafic and ultramafic rocks. Liquation, liquid immiscibility, settling out from magmas of sulfide, sulfide oxide, or oxide melt that accumulate beneath the silicates or injected into wall rocks or in rare cases erupted on the surface (e.g., Naldrett, 2010; Macheyeki, 2011; Ridley, 2013; Heinrich and Candela, 2014; Moon, 2016). Generally, the Ni−Cu deposits are usually associated with PGE as by-products (Naldrett, 1997, 2004).

2. Deposits formed from immiscible sulfide melt phases: PGE sulfide deposits (Ridley, 2013). Economic PGE primary deposits of this type are laterally extensive as thin layers or reefs, from less than 1 m thick to about 20 m thick in layered ultramafic to mafic large-volume and extensive intrusions in the upper crust. The reefs are broadly parallel to the cumulate layering, and are continuous along much of the extent of the exposed intrusions. There may be multiple reefs at different levels in one layered intrusion. Excluding by- and coproduct PGE resources of Ni−Cu sulfide deposits, almost all known economically significant PGE resources are in three exceptionally large intrusions more than about 4 km thick ($>10{,}000\ km^3$ volume), which have repeated multiple cycles of rhythmic cumulate layering and reversals of composition trends of cumulate minerals of layers of the Great Dyke of Zimbabwe (Naldrett, 1997; Mason-Apps, 1998; Naldrett, 2004; Ridley, 2013).

   The segregation of sulfide melt from silicate melt and the immiscibility of sulfide phases are actually promoted by tectonic activities. Both Ni−Cu and PGE, that is, Ni−Cu (PGE) deposits can be well understood and appreciated when looked at a global scale and therefore anticipated that this interplay of tectonics with the dynamic behavior of magmatic systems will become increasingly recognized, and has important implications for deposit exploration (Figs. 2.1 and 2.2; Begg et al., 2018).
3. Deposits formed from low-degree (small fraction) partial melting of mantle (Ridley, 2013; Heinrich and Candela, 2014). The partial melting of a small fraction of a mantle leads to deposition of LREE in carbonatites (e.g., Yang and Santosh, 2015).
4. Deposits formed through the incorporation of a mineral from depth in the earth into magma: diamond deposits in kimberlites and

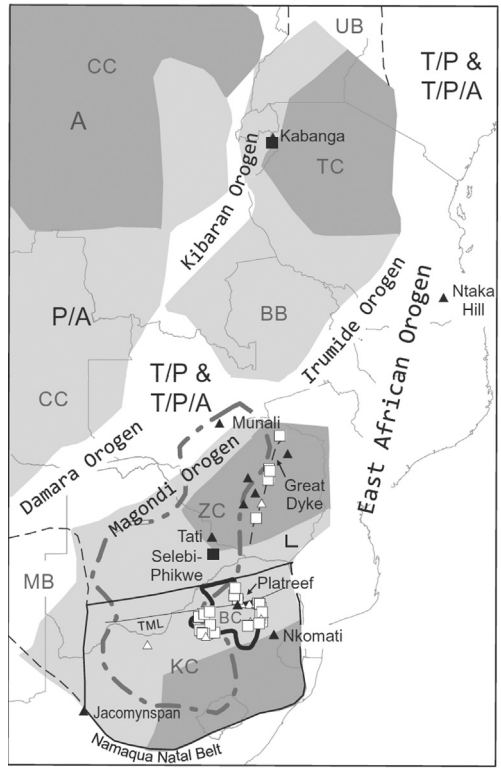

FIGURE 2.1 Deposits and lithospheric resilience. Relationship of giant (squares) and major (triangles) Ni–Cu(-PGE; black) and PGE (white) deposits of Africa with respect to archons (A), proton/archons (P/A), and intervening areas of tecton/proton (T/P) and tecton/proton/archon (T/P/A). Deposits are preferentially located within, or at the margins of the most resilient lithosphere (A, P/A). Thin black lines outline the Kaapvaal Craton and the internal paleocraton boundary represented by the TML. The high-velocity SCLM root at 100–175 km depth (thick gray dash-dot line) is taken from the updated 2011 seismic tomography model of Grand (2002). Note the position of the Great Dyke (dashed line) along the edge of this anomaly, suggestive of a paleocraton boundary. *BB*, Bangwelu block; *BC*, Bushveld complex (thick black outline); *CC*, Congo Craton; *KC*, Kaapvaal Craton; *L*, Limpopo Belt; *MB*, Maltahohe block; *TC*, Tanzania craton; *UB*, Ugandan block; *ZC*, Zimbabwe craton (Begg et al., 2018).

lamproites (Ridley, 2013; Fig. 2.3). It is the process responsible for the formation of diamond in Kimberlites (Republic of South Africa, Canada, Tanzania, etc.). This process also leads to the formation of strongly alkaline silicate igneous rocks such as in the Kola alkaline province of the Russian Federation (e.g., Petrov, 2004; Heinrich and Candela, 2014).

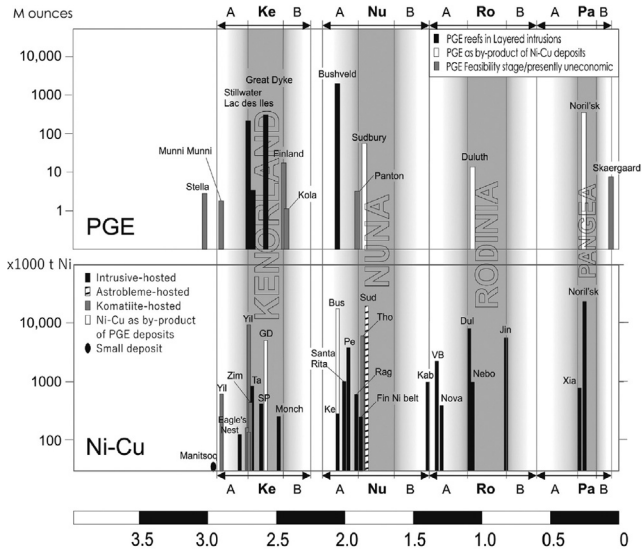

FIGURE 2.2 Secular distribution of PGE and Ni–Cu deposits and key elements of the supercontinent cycle. Supercontinent peaks Kenorland, Ke, Nuna, Nu, Rodinia, Ro, and Pangea, Pa, are preceded by periods of amalgamation, A, and dispersed during periods of breakup, B. Komatiitic-hosted (high-MgO) deposits are restricted to the earlier two supercontinent cycles. Note the clustering of deposits about the amalgamation and peak stages. *Bus*, Bushveld; *Dul*, Duluth; *Fin Ni belt*, Finnish Ni belt; *GD*, Great Dyke; *Jin*, Jinchuan; *Kab*, Kabanga; *Ke*, Keivitsa; *Monch*, Monchegorsk; *Nebo*, Nebo–Babel; *Pe*, Pechenga; *Rag*, Raglan; *SP*, Selebi Phikwe; *Sud*, Sudbury; *Ta*, Tati; *Tho*, Thompson; *VB*, Voisey's Bay; *Xia*, Xinjiang Province deposits (including Huangshandong, Huangshan, Kalatongke, Xiangshan); *Yil*, Yilgarn; *Zim*, Zimbabwe (Begg et al., 2018). Source: *Modified after Maier, W.D., Groves, D.I., 2011. Temporal and spatial controls on the formation of magmatic PGE and Ni-Cu deposits. Mineralium Deposita 46, 841–858.*

These deposits are formed through extreme fractionation of magma: rare-metal pegmatites (Ridley, 2013; Heinrich and Candela, 2014; Dill, 2015, Fig. 2.4). The principle of magmatic fractionation and therefore enrichment/depletion of partial elements obeys the equation (Robb, 2005):

$$\frac{C_{\text{liq}}}{C_{\text{o}}} = \frac{1}{D_{\text{res}} + F(1 - D_{\text{res}})} \tag{2.1}$$

where C_{liq} is the concentration of a trace element in the liquid (melt); C_{o} is the concentration of trace element in parental (unmelted) solid; D_{res} is the bulk partition coefficient of the residual solid (after the melt is extracted); F is the weight fraction of melt produced (Rollinson, 1993, 2012).

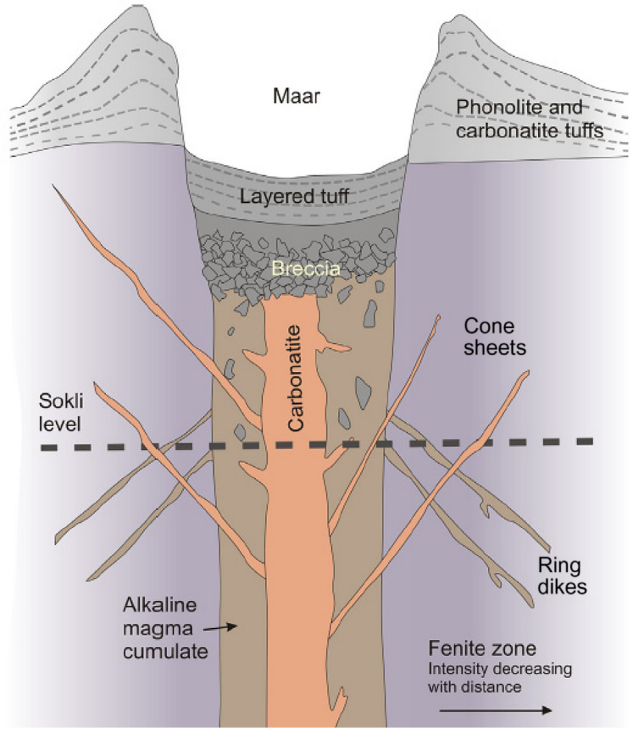

FIGURE 2.3 Cross section of a standard carbonatite, with Sokli erosion level estimated (O'Brien, 2015).

It should be noted that the extraction of a partial melt from its residue, whether it be from an igneous or sedimentary protolith, is a process that segregates chemical components (i.e., fractionation). Partial melts can be considerably enriched in certain elements, but depleted in others, relative to the source rock (Robb, 2005). Pegmatites are enriched with elements that are mostly lithophiles and include the large ion lithophile (LILEs) (Li, Rb, Cs, Be), high field strength elements (HFSEs) (Ga, Sn, Hf, Nb, P, Ta, Y, U, Th, REEs), and strongly soluble elements in aqueous solutions (B, F). Examples of currently or recently exploited pegmatites include: Rössing, Namibia for U (Berning et al., 1976); Tanco, Manitoba, Canada for spodumene, Cs, Ta (Černý et al., 1996); Volta Grande, Brazil; Kenticha, Ethiopia; and Green bushes and Wodgina, Western Australia for Sn, Ta (Partington, 1990).

Hydrothermal deposits are deposits from hot aqueous solution (enrichment by selective dissolution, transport, and precipitation, e.g., Heinrich and Candela, 2014), which may have had a magmatic, metamorphic, surface, or other sources (Robb, 2005). In other words for the

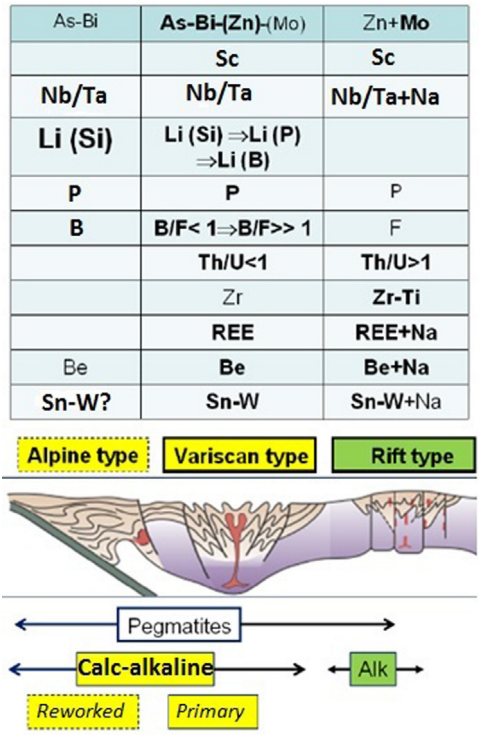

FIGURE 2.4 Rare element pegmatites and the geodynamic setting (CMS classification scheme—chemical qualifiers). The size and font of the letters are used to demarcate the significance of each element in the various settings. Bold-faced means widespread occurrence, set in brackets or added up with a quotation mark means minor potential as to the accumulation of a certain element or concentration processes uncertain. Source: *From Dill, H.G., 2015. Pegmatites and aplites: their genetic and applied ore geology. Ore Geol. Rev. 69, 417–561. Available from: https://doi.org/10.1016/j.oregeorev.2015.02.022.*

metals to be precipitated, they must have been selectively dissolved. How many metals are selectively dissolved is the function of several factors including the nature of metal–ligand complexes that can be formed (Robb, 2005), a process that can be well described by the Pearson's principle.

The Pearson's principle states that in a competitive situation, hard metals (acids or electron acceptors) will tend to complex with hard ligands (bases or electron donors), and soft metals with soft ligands. The Li^+, Na^+, K^+, Rb^+, Cs^+ for example, are hard metals, whereas Au^+, Ag^+, Cu^+ are the soft metals and Zn^{2+}, Pb^{2+}, Fe^{2+} are the divalent transition metals or borderline metals (Robb, 2005). Other hard metals described in Robb (2005) include Be^{2+}, Sr^{2+}, Ba^{2+}, Fe^{3+} and Ce^{4+}, Sn^{4+}, Mo^{4+}, W^{4+}, V^{4+}, Mn^4 and soft metals include Hg^{2+},

TABLE 2.3 Ligands occurring in hydrothermal ore solutions (Seward et al., 2014).

Hydroxide	OH^-
Halide ions	F^-, Cl^-, Br^-, I^-,
Sulfur species	HS, Sn, SnS^{2-}, $SO3^{2-}$, $S_2O_3^{2-}$, SO_4^{2-}
Ammonium (ammine)	NH3
Oxyanions	CO_3^{2-}, PO_4^{3-}, ASO_3^{3-}, SbO_3^{3-}, MoO_4^{2-}, WO_4^{2-}, SiO_4^{4-}
Thioanions	AsS_3^{3-}, SbS_3^{3-}, MoS_4^{2-}, WS_4^{2-}
Carboxylates	CH_3COO^- (acetate), $C_2H_5COO^-$ (propionate), $CH_2(COO)_2^{2-}$ (malonate), $(COO)_2^{2-}$ (oxalate)
Miscellaneous ligands of possible interest	HTe^-, Te_2^{2-}, CN^-, SCN^-

Cd^{2+}, Sn^{2+}, Pt^{2+} Pd^{2+} and Hg^{2+}, Cd^{2+}, Sn^{2+}, Pt^{2+}, Pd^{2+}. An example of hard ligand is $OH^- - F^- - NO_3^- - HCO_3^- CH_3COO^-$, whereas $HS^- - I^- - CN^- - H_2SS_2O_3^{2-}$ is a soft ligand.

The ligands of interest in hydrothermal systems are shown in Table 2.3. These metals and ligands are described in terms of their hard–soft breakdown and how that relationship is applicable to ore-forming processes. The metal–ligand relationship provided above is simply an approximation of what is most likely to happen in the function of variables such as oxidation state, pH, temperature, and fluid composition (Robb, 2005). In nature, metals may complex with any base, most suitable available, thus the metal–ligand complex to be formed will be quite different to those predicted on theoretical grounds (Robb, 2005).

Brugger et al. (2016) show that apart from metal–ligand complexes being available for ore deposition, the ore transport and precipitation of metals are largely controlled by coordination chemistry of hydrothermal systems as shown in the periodic table for hydrothermal geochemistry in Fig. 2.5.

However, in economic geology, what is important is not just the formation of the metal but the formation of a viable ore deposit. It requires the presence of high fluid/rock ratios, as well as efficient precipitation mechanisms to take metals out of solution and concentrate them in the host rock (e.g., Seward and Barnes, 1997). For example, solutions that deposit Au and Ag are typically in the range 1 ppb to 1 ppm, than those associated with Cu, Pb, and Zn ores. In the latter case, massive sulfide deposits are formed from fluids that typically carry 1–100 ppm of metal, whereas the fluids associated with the MVT and PDs are relatively enriched with concentrations in the range 100–1000 ppm.

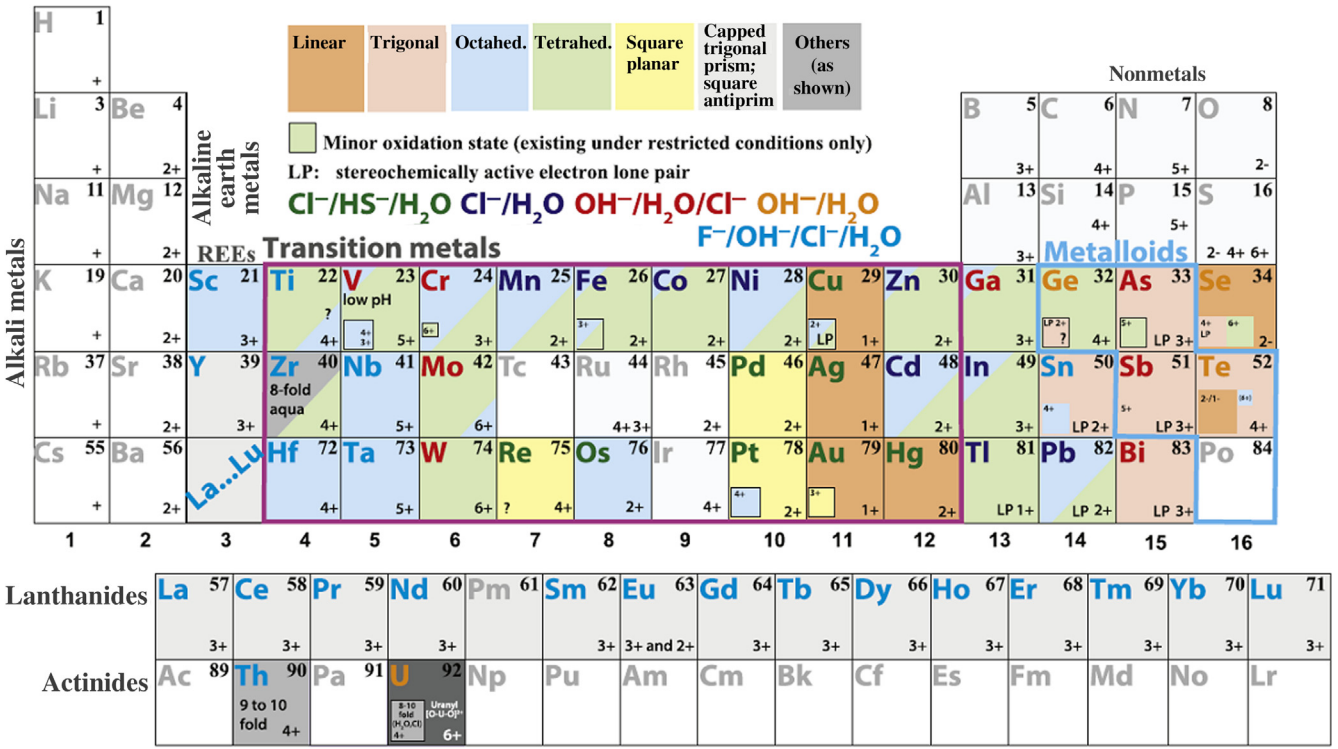

FIGURE 2.5 A periodic table for hydrothermal geochemistry showing coordination chemistry of metals in upper crustal geological fluids. Source: *From Brugger, J., Liu, W., Etschmann, B., Mei, Y., Sherman, D.M., Testemale, D., 2016. A review of the coordination chemistry of hydrothermal systems, or do coordination changes make ore deposits? Chem. Geol. 447, 219–253. Available from: https://doi.org/10.1016/j.chemgeo.2016.10.021.*

Skarn deposits (e.g., W, Cu, Au), PDs (e.g., "Cu, Mo porphyries") and vein deposits (e.g., Sn−W veins) are actually magmatic−hydrothermal deposits because they are caused by fluid saturation of H_2O-bearing magmas (Heinrich and Candela, 2014). Other examples of hydrothermal deposits include Epithermal veins and breccias that are due to continental geothermal systems (i.e., shallow magmatic fluids), Iron oxide hosted Cu−Au−U−REE ("IOCG") deposits caused by continental magmatic fluids interacting with evaporitic brines, volcanic-hosted massive sulfide deposits due to seawater convection through oceanic crust, orogenic ("mesothermal") gold−quartz veins due to metamorphic dehydration of deep magmatic fluids, sediment-hosted Cu ± Co deposits and stratiform Pb−Zn−Ag deposits ("sedex" = sedimentary−exhalative), caused by basin brines: connate or meteoric water + evaporites (Heinrich and Candela, 2014). Other examples of hydrothermal deposits due to basin brines are the MVT Pb−Zn + epigenetic replacement in carbonates ± sandstones. Uranium in sandstones ("roll-front U deposits") and vein—and "unconformity-related U deposits" are also hydrothermal deposits caused by deep infiltration of oxygenated surface waters.

1. Deposits due to lateral secretion. In this type of deposits, ore- and gangue-forming materials from the country rocks diffuse into faults and other structures (Moon, 2016).

Pyrometasomatic deposits are formed by both magmatic and hydrothermal processes, that is, magmatic−hydrothermal ore-forming processes. These deposits can be facilitated by some physical and chemical properties of water such as magmatic−hydrothermal fluids, water solubility in magmas, and first boiling and second boiling of granite-related magmatic−hydrothermal ore deposits. Minerals in this group include porphyry Cu, Mo, and W deposits, polymetallic skarn deposits, and epithermal Au−Ag−(Cu) deposits (Fig. 2.7). Generally, Magmatic−hydrothermal deposits are the sole producers of global Cu, Mo, Sn, W, In, and Re, and are a significant source of Au, Ag, Pb, Zn, and other minor and rare metals (Heinrich and Candela, 2014). Summarized geological context of PD and epithermal ore deposits are shown in Fig. 2.6.

Regions that experienced such kind of deposits include the magmatic−hydrothermal fluids associated with granite intrusions of the La Escondida porphyry Cu deposit in Chile, the MacTung W skarn deposit in Yukon−Canada, and magmatic−hydrothermal fluids in volcanic environments such as the high- and low-sulfidation epithermal gold deposits of Kyushu, Japan and Witwatersrand Basin gold deposit, in South Africa (Tucker et al., 2016).

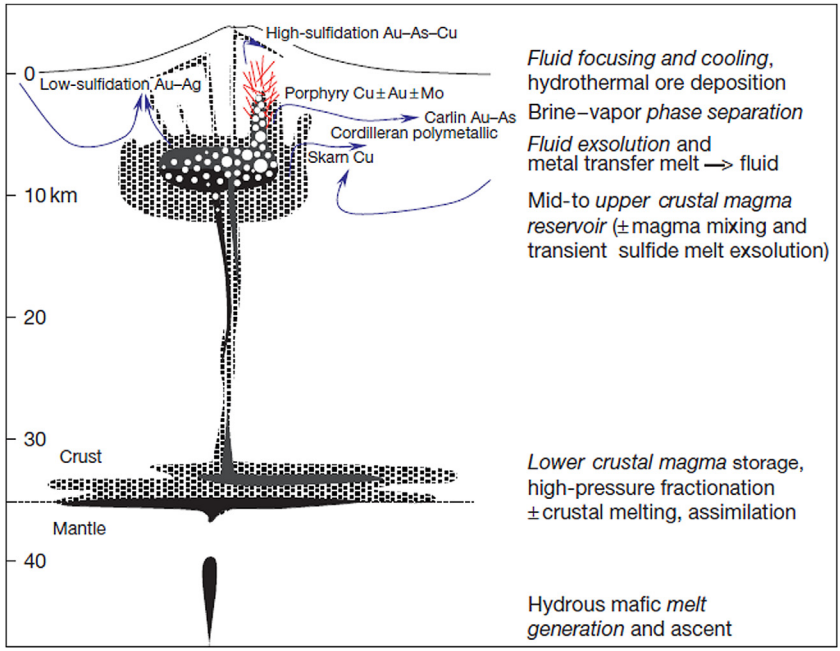

FIGURE 2.6 Schematic illustration of the geological components, ore types, and processes in crustal-scale magmatic–hydrothermal systems. Porphyry copper deposits form in a dense network of hydrofractures (red) around dikes and stocks above the roof of hydrous magma chambers, by precipitation of sulfides and gold from single phase or more commonly two-phase fluids of coexisting hypersaline liquid (brine) and vapor. Au-rich varieties predominate at shallow levels (1–3 km below surface) while porphyry deposits formed as deep as 8 km are generally Cu ± Mo dominated and Au-poor. Copper ± Zn ± Au skarns, Cordilleran vein, and replacement Cu–Zn–Pb–Ag ± Au deposits, and Carlin-type Au deposits rich in arsenious pyrite are hosted by carbonate-bearing sedimentary host rocks controlling pH by carbonate dissolution; they form at decreasing temperatures and increasing distance from magmatic intrusions. Carlin-type gold deposits are additionally characterized by abundant organic carbon in the host sediments. Their formation temperature and the low salinity of ore fluids with liquid-like density overlap with fluid properties in other epithermal precious metal deposits. High-sulfidation epithermal deposits are characterized by intense acid leaching and sulfate and clay alteration caused by hot low-density magmatic vapor, typically preceding the main stage of ore deposition by low-salinity aqueous liquid. Low-sulfidation epithermal deposits are generally more distal to intrusions and are characterized by near-neutral fluids causing feldspar–muscovite alteration, with a greater proportion of convecting meteoric water and a less obvious magmatic fluid input. Source: *From Heinrich, C.A., Candela, P.A., 2014. Fluids and ore formation in the Earth's crust. In: Treatise on Geochemistry, pp. 1–28.*

2.1.2.4 *Deposits due to external surface processes*

Ore deposits in this category can be due to mechanical accumulation, sedimentary precipitates, residual processes, secondary supergene environment, and volcanic exhalative (=sedimentary exhalative):

- Deposits due to mechanical accumulation: This is due to the concentration of heavy, durable minerals into placer deposits (Guilbert and Park, 1986). Examples of minerals deposited by this process are rutile–zircon sands, Tin placers, gold placers, industrial sands, gravels, and kaolin deposits (Moon, 2016).
- Deposits due to sedimentary precipitates: This is due to precipitation of particular elements in suitable sedimentary environments, with or without the intervention of biological organisms (Westphal et al., 2010). Minerals deposited by this process include banded iron formation of Precambrian shields, Mn deposits, evaporite deposits, and phosphate deposits (e.g., Moon, 2016).
- Deposits due to residual processes: These are due to soluble elements in the remaining material are leached from rocks and get deposited somewhere where they form deposits (Guilbert and Park, 1986). Examples of minerals deposited by this process include gossan deposits of Ni laterites, bauxites, and kaolin deposits (Moon, 2016).
- Deposits due to secondary supergene environment: These kinds of deposits are made possible by leaching of valuable elements from the upper parts of mineral deposits and their precipitation at depth to produce higher concentrations. Examples of minerals in this subcategory include many gold and silver bonanzas and the upper parts of a number of porphyry copper deposits (e.g., Robb, 2005; Moon et al., 2006).
- Deposits due to volcanic exhalative (=sedimentary exhalative): These kinds of deposits are due to exhalations of hydrothermal solutions at the surface, usually under marine conditions and generally producing stratiform ore bodies (Robb, 2005). Examples are base metal deposits of Megagan, German; Kuroko deposits of Japan; and Solfatara deposits (kaolin + alunite).

2.1.3 The role of global tectonics and geological time in the formation of ore deposits

Global tectonics is the second major factor in the formation of distinct ore deposit types and a key to understanding their spatial and secular distribution (Groves et al., 2005; Holland, 2005) as most hydrothermal environments where ores deposits are formed are commonly found in many active, continental, and oceanic geothermal fields along plate tectonics margins (Barnes, 2015). Thus chromium deposits form by physical accumulation of what is usually an accessory mineral (chromite, $FeCr_2O_4$) from large reservoirs of mafic magma. Such magma chambers either form as intraplate layered intrusions (possibly related to mantle plumes) or at spreading axes in the oceanic domain (Stowe, 1994).

The world porphyry Cu–Au belt, for example, is restricted within recent converging/subduction zones. Worldwide, Cu–Au mineralization seems to be restricted within ridge subduction zones that are characterized by adakitic rocks (Sun et al., 2010: 17). Porphyry Cu mineralization seems to be restricted in arc-related structures within the Phanerozoic. This coincides well with the ring of fire. The reason why plate boundaries are the locus of mineralization is that the energy released along boundaries, results in volcanic and hydrothermal activity that creates the right conditions for many minerals to be concentrated. Plate boundaries are also a way for deep-seated rocks from the mantle to find a way to the near-surface because these boundaries, as earlier on hinted, are the weak zones. These rocks become the source of many of our largest mineral deposits. Geologists therefore have to know how the plates move and predict where they could have been in the past—by having a clear understanding of the location of ancient plate boundaries, it is easier to predict where regional mineralization, and hence ore deposits may occur today (Arribas and Mizuta, 2018).

The ore deposit types with global tectonic settings are shown in Fig. 2.7. It should be noted however that global tectonics does not answer all questions related to ore deposits. In other words, location of mineralization on the crust is not necessarily the function of plate tectonics; in fact, some deposit types appear to require the absence of plate tectonics inasmuch as they form tectonically undisturbed regimes (Sangster, 1980). Examples include the MVT-type Pb–Zn deposits, sandstone U deposits, sedimentary barites, phosphates, and superior-type iron formations; they are not easily explained by global tectonics.

In summary, three groups of factors—transport medium, global tectonics, and the earth's changing climate and atmosphere—allow a first-order explanation for the range of major ore deposit types. Common to all ore-forming processes is the fact that selective element enrichment is an entropy-reducing process that requires a net input of energy. For a deeper understanding of the factors controlling ore formation, we therefore need to focus on the energy sources—that is, the physical and chemical driving forces—contributing to processes separating elements from each other on a large scale and with high efficiency (Heinrich and Candela, 2014) (Fig. 2.8).

2.1.4 Source of metals in ore deposits: principles

Understanding the source of metals of ore deposits is paramount as such knowledge can assist in predicting or locating similar mineralized parts of the earth's crust. Temperature, pressure, oxygen fugacity are important variables in understanding deposit genesis (Kotzer and

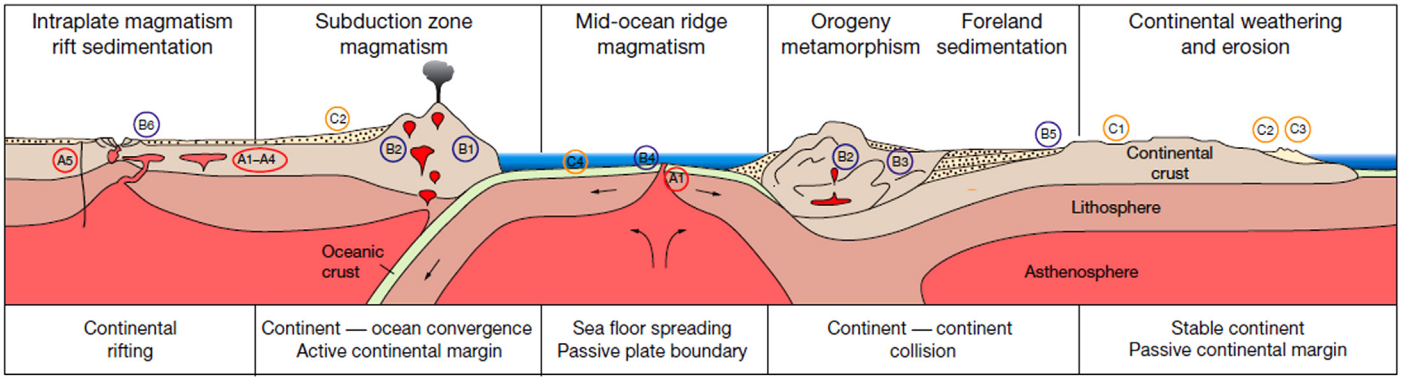

A: Magmatic ore deposits

A1. Chromitites as (ultra-)mafic cumulates in layered intrusions and ophiolites

A2. V-magnetite in mafic intrusions (V, Ti)

A3. Pegmatites (Li, Cs, Be, Nb, Ta)

A4. Ni- und PGE-sulfide deposits in mafic intrusions und flood basalts

A5. Carbonatite (REE) and kimberlite (diamond) deposits

B: Hydrothermal ore deposits

B1. Porphyry Cu (Mo, Au) and epithermal Au, Ag (Hg, ...) deposits

B2. Sn-W veins and greisens in granites

B3. Orogenic ("metamorphogenic") Au-quartz vein deposits

B4. Volcanogenic massive sulfides (Cu, Zn)

B5. Sediment-hosted (MVT, 'sedex') Pb, Zn, Cd, Cu, Co deposits

B6. Sandstone-hosted and unconformity-related U (V, F, Mo, Au, PGE) deposits

C: Surface-related ore deposits

C1. Residual ore deposits: bauxite (Al), Ni-laterite deposits

C2. Alluvial placer deposits (Sn, Ta, Au; U)

C3. Beach-sand placers (Ti, Zr, REE)

C4. Manganese nodules and crusts on the ocean floor (Mn, Co, Ni, Cu...)

FIGURE 2.7 Schematic illustration of the recurrent association of ore deposit types with global tectonic settings, including active and passive continental margins, oceanic spreading centers including back-arc basins, as well as land surfaces, sedimentary basins, and hot spots in the interior of lithospheric plates. Labels A, B, C refer to major metal-transporting media and ore deposit types in Table 2.3. Source: *From Heinrich, C.A., Candela, P.A., 2014. Fluids and ore formation in the Earth's crust. In: Treatise on Geochemistry, pp. 1–28.*

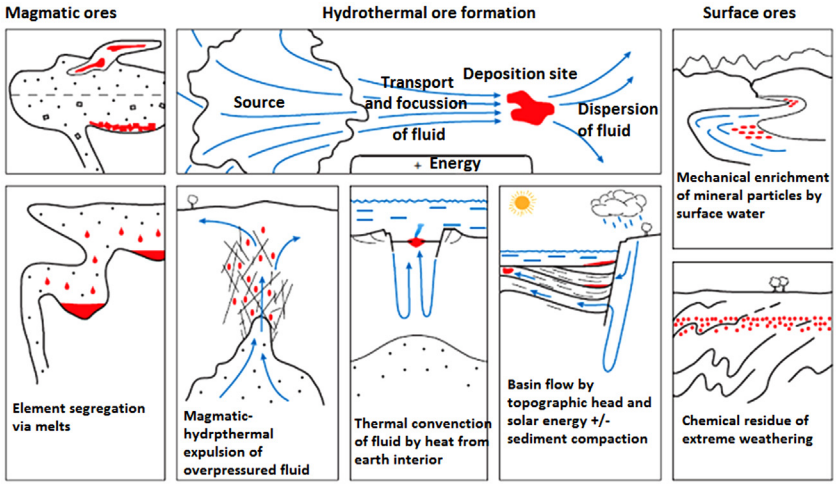

FIGURE 2.8 Schematic illustration of three principal processes of selective element enrichment that can produce mineral deposits in the earth's crust, grouped by the main agent of material transport: magmatic melts, hydrothermal fluids, or surface waters (Kesler, 1994). Source: *From Heinrich, C.A., Candela, P.A., 2014. Fluids and ore formation in the Earth's crust. In: Treatise on Geochemistry, pp. 1–28.*

Kyser, 1995). Isotopic studies (Kotzer and Kyser, 1995; Legros et al., 2019), fluid inclusions (Richard et al., 2013; Brugger et al., 2016; Kyser, 2016; Xiong et al., 2018), and trace element geochemistry are important aspects to be considered in studying deposit genesis (e.g., Robb, 2005; Mungall, 2014). The principles underlying these studies, particularly those on geochemical techniques, are briefly discussed in this subchapter.

2.1.4.1 *Pressure, temperature, chemical composition, and oxygen fugacity*

Pressure, temperature, chemical composition, and oxygen fugacity ($fO2$) are critical parameters useful in understanding ore deposit characteristics and processes that lead to ore generation and they can assist in identifying correct environment (s) for exploring potential minerals (Legros et al., 2019). In the context of chemical composition for example, most highly evolved alkaline intrusives do not host uranium deposits because they do not evolve to concentrate uranium in their differentiates (Kotzer and Kyser, 1995; Richard et al., 2013; Xiong, et al., 2018).

Regarding oxygen fugacity, Kress and Carmichael (1991) show that the Fe_2O_3/FeO ratio of melts is linked to its oxygen fugacity and can be estimated by the empirical relationship:

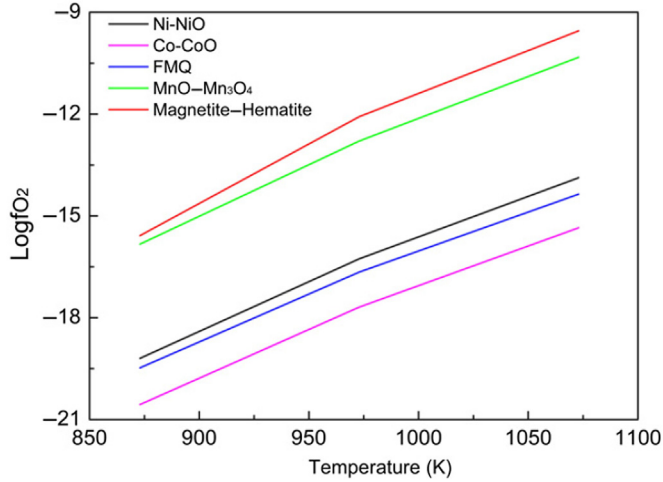

FIGURE 2.9 Fugacity–temperature diagram. Log *f*O2, versus T at 1 bar P for common buffer assemblages. MH, NiNiO, FMQ, WM, IW, and QIF are respectively magnetite–hematite, nickel–nickel oxide, fayalite–magnetite–quartz, wüstite–magnetite, iron–wüstite and quartz–iron–fayalite (e.g., Chou, 1978; Lindsley, 1991; Frost et al., 1988). Source: *From Sun, W., Huang, R., Li, H., Hu, Y., Zhang, C., Sun, S., et al., 2015. Porphyry deposits and oxidized magmas: a review. Ore Geol. Rev. 65, 97–131.*

$$\log\left(fO2\right) = \log\left\{\exp\left[\frac{\left(\frac{\ln(Fe_2O_3)}{FeO}melt - \frac{b}{T} - c - \sum_i^n diXi\right)}{a}\right]\right\} \qquad (2.2)$$

where $a = 0.207$; $b = 12{,}980$; $c = -6.115$. Temperature T is in Kelvin and Xi is between 0 and 1 calculated from oxides as wt.% (Liao et al., 2016).

Further, in silicate magma and in ideal cases, oxygen fugacity is equal to its partial pressure (e.g., Evans et al., 2017) and positively correlated with temperature, T (Lindsley, 1991). Fig. 2.9 illustrates how oxygen fugacity can be related to mineral assemblage buffers such as fayalite–magnetite–quartz (FMQ), nickel–nickel oxide, that is, Ni–NiO, wüstite–magnetite (WM), iron-wüstite (IW); quartz–iron–fayalite (QIF), and hematite–magnetite (e.g., Chou, 1978; Lindsley, 1991; Frost et al., 1988; Ablay et al., 1998).

Mineral assemblage buffers are assemblages of minerals or compounds that constrain oxygen fugacities as a function of temperature (Lindsley, 1991). If a rock contains pure minerals that constitute a redox buffer (e.g., magnetite–hematite, nickel–nickel oxide, FMQ, WM, IW, QIF), then the oxygen fugacity of equilibration is defined by one of the curves in Fig. 2.9 (Chou, 1978; Lindsley, 1991; Frost et al., 1988). For other rocks with suitable minerals, oxygen fugacities can be calculated, and the redox

conditions that are obtained from calculation be compared by the fugacity–temperature diagram in Fig. 2.9 (e.g., Lindsley, 1991).

Oxygen fugacity strongly influences the crystallization sequences and composition of crystallizing minerals (Liao et al., 2016). Preservation of diamonds during transport from the mantle to the surface is estimated by assessing the oxygen fugacity of the magma (Moon et al., 2006). Highly oxidized intrusions and economic ore deposits are commonly associated with relatively higher oxygen fugacity values (Trail et al., 2012; Zhou et al., 2018). For example, the oxygen fugacity value of ΔFMQ +2 averaging between +4.50 and +7.12 is associated with medium-sized to super large-sized porphyry Mo deposits in the East Xing'an–Mongolian Orogenic Belt and below which the deposits are small (Zhou et al., 2018). It should be emphasized here that not all mineral deposits are associated with increase in oxygen fugacity as some minerals would be deposited when oxygen fugacity decreases. This is because oxygen fugacity is not the only control of mineral deposition (e.g., Chou, 1978). Other factors that control mineral deposition are pressure, temperature pH, Eh, sulfur fugacity, etc. (Fig. 2.10). For example, gold mostly occurs as $AuCl_2^-$ in a system with temperature higher than 400°C (Gammons and Williams-Jones, 1997; Zhu et al., 2011), but as temperature decreases (the primary mechanism), gold is deposited (Zhu et al., 2011). At lower temperatures, $Au(HS)_2^-$ is the dominant

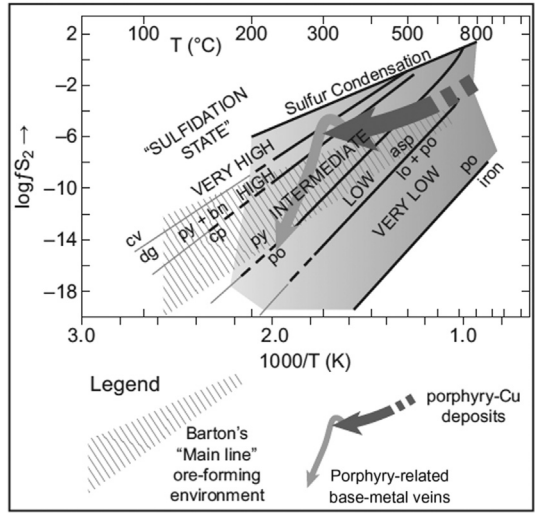

FIGURE 2.10 Evolution curves of the hydrothermal or "ore-forming" fluids. Shown are sulfidation equilibrium curves for common ore-forming minerals. Source: *Kretschmar, U., McBride, D., 2016. Understanding hydrothermal Systems, In Ulrich Kretschmar and Derek McBride (eds), The Metallogeny of Lode Gold Deposits, pp 151–198, First Edition Elsevier, 345p.*

phase, and the maximum solubility exists in the vicinity of the $H_2S - HS^- - SO_4^{2-}$ equilibrium point and with the decline of oxygen fugacity, the Au–S complex breaks down leading to gold precipitation (Cooke and Simmons, 2000; Robb, 2005; Zhu et al., 2011):

$$2Au(HS)_2^- + H_2O \rightarrow 2Au + 4HS^- + 2H^+ + 0.5O_2$$

$$2Au(HS)_2^- + 8H_2O \rightarrow 2Au + 4SO_4^{2-} + 4H^+ + 8H_2$$

$$FeCO_3 + Au(HS)_2^- = FeS_2 \text{ pyrite} + CO_2 + H_2O + Au \text{ (Zhu et al., 2011)}$$

Iron sulfides monitor the sulfur fugacity just like how Fe–Ti oxides monitor oxygen fugacity in rocks (Frost and Frost, 2014). With increasing temperature, or at low sulfur fugacities, pyrite breaks down to pyrrhotite by the reaction:

$$(1 - x)\,FeS_2 = Fe(1 - x)S + \left(\frac{1}{2 - x}\right) S_2 \tag{2.3}$$

This relationship indicates that, whereas pyrite may be stable in some relatively low-temperature rocks such as granites, pyrrhotite is the only sulfide found in high-temperature rocks such as basalt and gabbro.

The concentration of gold in potentially ore-forming solutions is a function of the distribution of sulfur species. For temperatures of 200°C–400°C, pressures of 200 MPa and near-neutral pH, $Au(HS)_2$—is the dominant gold–hydrosulfide complex (Shvarov and Bastrakov, 1999; Phillips and Evans, 2004). Thus sulfur is one of the key elements trapped in fluids during movements of hydrothermal fluids as a function of temperature, pressure, and pH (e.g., Phillips and Evans, 2004; Frost and Frost, 2014). Trisulfur ion, (S^{-3}), recently discovered in laboratory experiments (Pokrovski and Dubessy, 2015), may account for up to 10% of total dissolved sulfur (S_{tot}) at 300°C–500°C in fluids from arc-related magmatic–hydrothermal systems, and more than 50% S_{tot} at 600°C–700°C in S-rich fluids produced via prograde metamorphism of pyrite-bearing rocks (Steudel and Steudel, 2013; Pokrovski and Dubessy, 2015). In addition, the trisulfur ion may favor the mobility of sulfur itself and associated metals (Au, Cu, Pt, and Mo) in geological fluids over a large range of depth and provide the source of these elements for orogenic Au and porphyry–epithermal Cu–Au–Mo deposits (Chivers, 1974; Steudel and Steudel, 2013; Pokrovski and Dubessy, 2015).

2.1.4.2 *Fluid inclusions*

Fluid inclusions are microscopic pockets of gas or liquids trapped within minerals (Craig and Vaughan, 1981; Sun et al., 2015; Corral et al., 2017; Fig. 2.11). The pockets may contain information on the original

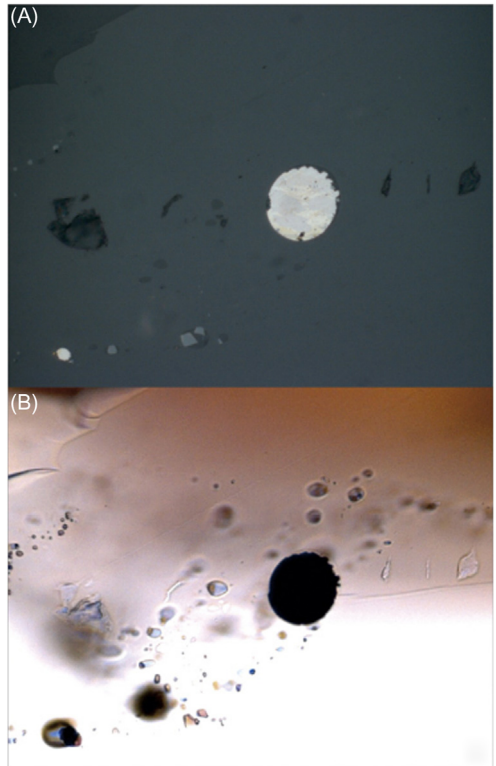

FIGURE 2.11 Images of sulfide inclusion in an olivine phenocryst of Manus glass under (A) reflected light and (B) and transparent light. Only one big sulfide globule is clearly identified under reflected light, which seemingly indicates sulfide saturation. This grain is actually associated with fluid inclusions as shown under transparent light. The unique composition of sulfides in Manus glasses (low Ni, Pt, etc.) may be plausibly interpreted by sulfides crystallized from magmatic fluids (Sun et al., 2015).

physical and chemical conditions at which the source rock was formed (e.g., Viter et al., 2013) and how the transportation–deposition mechanism of ore-forming fluids (in hydrothermal deposits) acted (Bodnar et al., 2014). The fluid inclusions can also constrain geochemical models used to investigate geochemical processes (Bertelli et al., 2009). Fluid inclusions, when trapped within crystals during initial growth from solution or during total recrystallization, are called primary inclusions or if recrystallization of the fluid inclusions is localized along fractures at some later time, they are referred to as secondary inclusions (Craig and Vaughan, 1981). In fluid inclusion studies therefore the fundamental task is to study the nature of fluids included or trapped by the minerals during alteration and mineralization processes (Trail et al., 2009, 2012; Xiong, et al., 2018).

2.1.4.3 *Radiogenic and nonradiogenic (stable) isotopes*

Isotopes are used in bedrock geology, archeology, forensics, food and beverage industry, and environmental sciences. The focus of this book and in particular this subchapter is on the application of isotopes in the field of geology, more especially in understanding the geodynamics of rocks, the ore deposit sources, and age of rocks and their associated mineral deposits.

The U–Pb (from sphalerite) and Re–Os (from molybdenite) are examples of sets of radiogenic elements that can be used to understand the geodynamic setting of some mineral deposits (e.g., Robb, 2005; Dai et al., 2009) and their age when properly employed. For instance, Dai et al. (2009) use the stable isotopes of sulfur ($\delta^{34}S$: 3.3‰–8.0‰) to predict that a mixed crust–mantle system was responsible for the metal ore source in the Mo (Fe) deposit Xiaojiayingzi, China. Furthermore, using the same data, they propose an early stage of subduction of the Paleo-Pacific plate beneath the Eurasian Block as related to the geodynamic setting of that deposit. Casa et al. (2003) employ a similar approach in determining the source of gold in Central Italy. They propose that the origin of gold in Ponte San Pietro deposit may be related to leaching of metapelites/phyllites derived from pelitic rocks containing some amount of sulfur-bearing organic matter. The Co, Ni, Mn, as well as the $\delta^{34}S$ data ($\delta^{34}S$ values of up to 7.0‰), suggest a different origin for the phyllite-hosted marcasite, the Ponte San Pietro quartz-vein-hosted pyrite, and for gold occurrences (see Table 2.4).

TABLE 2.4 Distribution of elements, element ratios, and $\delta^{34}S$‰ in marcasite within phyllites of the Verrucano formation (T–D samples) and in vein-hosted pyrite from Ponte San Pietro deposit, Central Italy.

Sample	Au	Co	Ni	Mn	As	Co/Ni	$\delta^{34}S$‰
T-D1	424	41	56	390	236	0.73	+ 2.5
T-D2	54	43	62	400	182	0.69	+ 7.0
T-D3	338	45	60	300	187	0.75	nd
T-E3	7400	Nd	nd	nd	nd	nd	+ 0.8
T-E4	1400	26	26	10	7500	1.0	+ 1.9
T-E5	2000	32	22	8	8500	1.45	nd
T-E6	17,000	47	29	13	71,000	1.62	nd
T-E8	21,000	28	18	16	8100	1.55	nd

Element values are given in ppm, except for Au in ppb, *nd*, not determined.
From Casa, G.D., Manni, A., Saviano, G., Violo, G., 2003. Gold occurrence in Central Italy—the Ponte San Pietro mineralization. Ore Geol. Rev. 23, 99–105. Available from: https://doi.org/10.1016/S0169-1368(03)00017-9.

The expression $\delta^{34}S = x‰$ means that ^{34}S is in parts per thousand and expressed relative to the most abundant sulfur isotope $\delta^{32}S$ (e.g., Ridley, 2013), that is:

$$\delta^{34}S = \left[\frac{\left(\frac{^{34}S}{^{32}S}\right)\text{sample} - \left(\frac{^{34}S}{^{32}S}\right)\text{standard}}{\left(\frac{^{34}S}{^{32}S}\right)\text{standard}}\right] \times 1000 \tag{2.4}$$

It is worth noting that in nature, the stable sulfur isotopes ^{32}S, ^{33}S, ^{34}S, and ^{36}S are approximately 95%, 0.75%, 4.2%, and 0.02%, respectively. The standard for sulfur isotope ratio stated in Eq. (3.3) is of iron meteorite and mantle-derived sulfur and has $\delta^{34}S$ values within a narrow range of 0% ± 1% (Ridley, 2013).

Isotopes of H and O can be used to tell about the origin of hydrothermal fluids as to whether or not they are from seawater, meteoric water, magmatic water, connate water, metamorphic water, or from mixed sources in the earth's crust that could have been responsible for the mineralization in question (e.g., Robb, 2005; Corral et al., 2017). The plot of hydrogen (δD permil) versus oxygen ($\delta^{18}O$ permil) isotopic ratios for various water types have been shown in Fig. 2.12. Note from that plot the linear meteoric water line ($\delta D = 8 \times \delta^{18}O + 10$) as well as the standard mean seawater values, standard mean ocean water (SMOW; δD permil = 0, $\delta^{18}O$ permil = 0). Thus one has to analyze from the ore samples, the values of δD and $\delta^{18}O$ and see where they plot in Fig. 2.12 for establishing the source of hydrothermal fluids. As it is always not easy to date the ore itself due to the absence of datable material, dating is done by using nonore materials associated with the ore. The plot of $^{143}Nd/^{144}Nd$ versus $^{87}Sr/^{86}Sr$ has been used by White and Patchett (1984) to characterize island arc volcanic materials of the South Sandwich, Lesser Antilles, Aleutians, Marianas, Philippines, Taiwan, Banda, and Sunda arcs (Fig. 2.13).

Further, the plot of $\delta^{18}O$ (‰) versus $\delta^{34}S$ (‰) for the Cerro Quema Au–Cu deposit (Azuero Peninsula, Panama) show that the fluid in the magmatic–hydrothermal system was sulfide dominant ($XH_2S = 0.69$) and the sulfur was of magmatic origin ($\delta^{34}S_{\Sigma S} = -0.5‰$) but that variable $\delta^{18}O$ at constant $\delta^{34}S$ of alunite and barite, and $\delta^{18}O$ values of fluids being in equilibrium with vuggy quartz (−2.3 to 3.1‰) suggest dilution of magmatic fluid by meteoric waters (e.g., groundwater) during alteration/mineralization (Corral et al., 2017). The $\delta^{13}C$ isotopic compositions for the DRC diamonds show values from −12.5‰ to −1.9‰ implying near mantle-like values (Kosman et al., 2016).

Deuterium–oxygen–carbon (D–O–C) isotopic systematics have been used by some scholars such as Aliyari et al. (2009) to study the hydrothermal deposits.

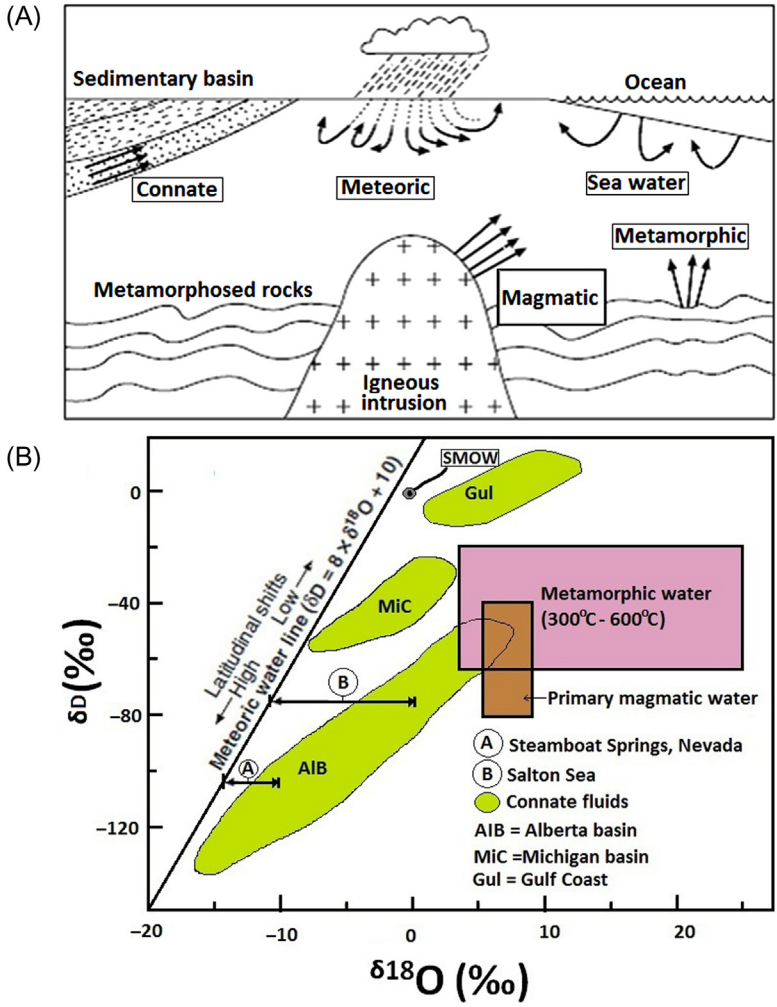

FIGURE 2.12 (A) The major types of liquid water that exist at or near the earth's surface. (B) Plot of hydrogen (δD permil) and oxygen ($\delta^{18}O$ permil) isotopic ratios for various water types. SMOW is defined to be zero for both δD and $\delta^{18}O$. Some ore-forming environments are clearly related to mixed fluid reservoirs; in the cases shown (see A and B) mixing of meteoric and connate fluids has taken place. Source: *After Taylor, H.P., 1997. Oxygen and hydrogen isotope relationships in hydrothermal mineral deposits. In: Barnes, H.L. (Ed.), Geochemistry of Hydrothermal Ore Deposits, third ed. John Wiley & Sons, New York, pp. 229–302. From Kretschmar, U., McBride, D., 2016. Understanding hydrothermal Systems, In Ulrich Kretschmar and Derek McBride (eds), The Metallogeny of Lode Gold Deposits, pp 151–198, First Edition Elsevier, 345p.*

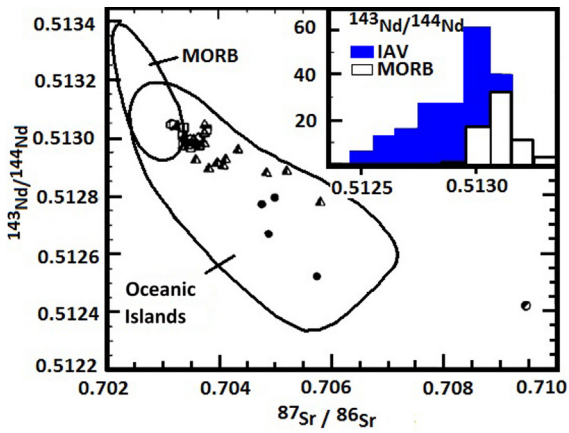

FIGURE 2.13 Nd–Sr isotopic data for Island Arc volcanic. Symbols are O = Aleutians, □ = New Britain, Δ = Marianas, ◪ = Izu, ● = Sunda, ▲ = Banda, and ◓ = Lesser Antilles. Inset refers to distinction in $^{143}Nd/^{144}Nd$ between mid-oceanic ridge basalts (MORB) and island arc volcanics (IAV) for all available analyses. Source: *From White, W.M., Patchett, J., 1984. HfNdSr isotopes and incompatible element abundances in island arcs: implications for magma origins and crust-mantle evolution. Earth Planet. Sci. Lett. 67 (2), 167–185. Available from: https://doi.org/10.1016/0012-821x(84)90112-2.*

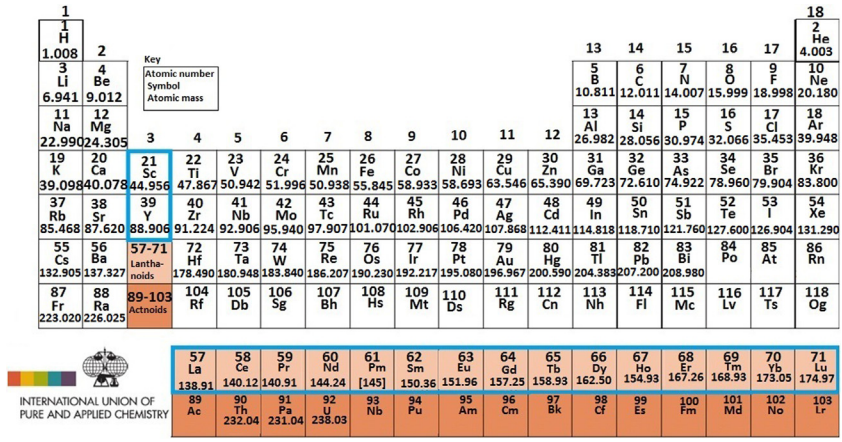

FIGURE 2.14 Periodic table of elements with rare earth elements, REE (LREE and HREE) shown in blue boxes. Source: *After Gaffney, J.S., Marley, N.A., 2018. Periodic table. In: General Chemistry for Engineers, 623. Available from: https://doi.org/10.1016/b978-0-12-810425-5.09983-5.*

2.1.4.4 *Rare earth elements*

2.1.4.4.1 Geochemistry and classification

REEs as indicated by blue boxes in Fig. 2.14 are a set of chemical elements in the periodic table, specifically the 15 lanthanides plus scandium

(Sc) and ythrium (Y), Sc, and Y are considered REE since they tend to occur in the same ore deposits as the lanthanides and exhibit similar chemical properties; their ability to readily discharge and accept electrons, make them indispensable and nonreplaceable in many electronic, optical, magnetic, and catalytic applications (e.g., Gaffney and Marley, 2018). Names of elements along with their symbols are shown in Table 2.5.

REEs are classified into two subgroups: LREEs comprising the first six elements of the Lanthanite series La, Ce, Pr, Nd, Pm, Sm (atomic numbers 57–62); and the heavy rare earth elements (HREE), comprising nine elements Eu, Gd, Tb, Dy, Ho, Er, Tm, Yb, Lu (with atomic numbers 63–71), and the 10th element ythrium despite its low atomic weight (Fig. 2.14), Y is classified with the HREE because its properties are closer to those of the HREE subgroup than to LREE (www.tasmanmetals.com/s/RareEarth.asp).

Despite their name, the REEs are in fact not especially rare. Each one of the REE is more common in the earth's crust than the elements Ag, Au or Pt, while Ce, Y, Nd, and La are more common than Pb (Fig. 2.14). Thulium and Lu are the least abundant REEs with crustal abundance of approximately 0.5 ppm.

The REEs, being capable of readily accepting and releasing electrons, are never found as free metals in the earth's crust and all their naturally occurring minerals consist of mixtures of various REEs with other metals and nonmetals. For example, garnet accommodates the HREE more than the LREE, and orthopyroxene and hornblende do so to a lesser degree. Sphene and plagioclase accommodate more LREE, and Eu^{2+} is strongly partitioned into plagioclase (e.g., Pun et al., 1997). Plotting concentration of the REE (normalized to mantle values) as the ordinate (y-axis) against increasing atomic number (as their degree of compatibility increases from left to right across the diagram), we can be able to characterize the genetic history of various rocks and ore deposits.

REE behave as incompatible elements, that is, they prefer magma over crystalline phases during crystal–liquid separation—be it partial melting or crystallization. As per Sen (2014), Sm and Nd behave as incompatible elements but Nd is slightly more incompatible than Sm. ^{143}Nd is a daughter isotope produced by α-decay of the radioactive isotope ^{147}Sm. Similar to the Sr system, Nd isotopic ratios are expressed in terms of $^{147}Sm/^{144}Nd$ (parent) and $^{143}Nd/^{144}Nd$ (daughter). Partial melting results in a greater Sm/Nd ratio of the residuum because Nd is more incompatible than Sm. It follows that as time progresses rocks crystallizing from such partial melts will evolve to lower $^{143}Nd/^{144}Nd$ than the residue because the residue will have a greater amount of $^{147}Sm/^{144}Nd$ ratio acquired during the partial melting event. Because of the differential change in Sm/Nd relative to Rb/Sr during partial

TABLE 2.5 Symbols of geochemical elements along with their names.

Atomic number	Element symbol	Name	Atomic number	Element symbol	Name
1	H	Hydrogen	60	Nd	Neodymium
2	He	Helium	61	Pm	Promethium
3	Li	Lithium	62	Sm	Samarium
4	Be	Beryllium	63	Eu	Europium
5	B	Boron	64	Gd	Gadolinium
6	C	Carbon	65	Tb	Terbium
7	N	Nitrogen	66	Dy	Dysprosium
8	O	Oxygen	67	Ho	Holmium
9	F	Fluorine	68	Er	Erbium
10	Ne	Neon	69	Tm	Thulium
11	Na	Sodium	70	Yb	Ytterbium
12	Mg	Magnesium	71	Lu	Lutetium
13	Al	Aluminum	72	Hf	Hafnium
14	Si	Silicon	73	Ta	Tantalum
15	P	Phosphorous	74	W	Tungsten
16	S	Sulfur	75	Re	Rhenium
17	Cl	Chlorine	76	Os	Osmium
18	Ar	Argon	77	Ir	Iridium
19	K	Potassium	78	Pt	Platinum
20	Ca	Calcium	79	Au	Gold
21	Sc	Scandium	80	Hg	Mercury
22	Ti	Titanium	81	Tl	Thallium
23	V	Vanadium	82	Pb	Lead
24	Cr	Chromium	83	Bi	Bismuth
25	Mn	Manganese	84	Po	Polonium
26	Fe	Iron	85	At	Astatine
27	Co	Cobalt	86	Rn	Radon
28	Ni	Nickel	87	Fr	Francium
29	Cu	Copper	88	Ra	Radium
30	Zn	Zinc	89	Ac	Actinium

(*Continued*)

TABLE 2.5 (Continued)

Atomic number	Element symbol	Name	Atomic number	Element symbol	Name
31	Ga	Gallium	90	Th	Thorium
32	Ge	Germanium	91	Pa	Protactinium
33	As	Arsenic	92	U	Uranium
34	Se	Selenium	93	Np	Neptunium
35	Br	Bromine	94	Pu	Plutonium
36	Kr	Krypton	95	Am	Americium
37	Rb	Rubidium	96	Cm	Curium
38	Sr	Strontium	97	Bk	Berkelium
39	Y	Yttrium	98	Cf	Californium
40	Zr	Zirconium	99	Es	Einsteinium
41	Nb	Niobium	100	Fm	Fermium
42	Mo	Molybdenum	101	Md	Mendelevium
43	Tc	Technetium	102	No	Nebelium
44	Ru	Ruthenium	103	Lr	Lawrencium
45	Rh	Rhodium	104	Rf	Rutherfordium
46	Pd	Palladium	105	Db	Dubnium
47	Ag	Silver	106	Sg	Seaborgium
48	Cd	Cadmium	107	Bh	Bohrium
49	In	Indium	108	Hs	Hassium
50	Sn	Tin	109	Mt	Meitnerium
51	Sb	Antimony	110	Ds	Darmstadtium
52	Te	Tellurium	111	Rg	Roentgenium
53	I	Iodine	112	Cn	Copernicium
54	Xe	Xenon	113	Nh	Nihonium
55	Cs	Cesium	114	Fl	Flerovium
56	Ba	Barium	115	Mc	Moscovium
57	La	Lanthanum	116	Lv	Livermorium
58	Ce	Cerium	117	Ts	Tennessine
59	Pr	Praseodymium	118	Og	Oganesson

Extracted from Fig. 2.14.

melting, the sign of the *epsilon* values for the Sm−Nd versus Rb−Sr systems means the opposite: positive $^{\varepsilon}$Nd value means depleted, whereas positive $^{\varepsilon}$Sr value means enriched composition (e.g., Sen, 2014; Kazemi et al., 2018).

Rocks from the primitive mantle have $^{\varepsilon}Nd = 0$ and $^{\varepsilon}Sr = 0$, whereas enriched igneous rocks have $^{\varepsilon}Nd < -2$ and $^{87}Sr/^{86}Sr > 0.705$ and depleted igneous rocks have $^{\varepsilon}$Nd of +6 to +10 and $^{87}Sr/^{86}Sr$ of 0.7025−0.703.

For kimberlites, although both Group 1 and Group 2 Kimberlites contain both compatible and incompatible elements, they can be distinguished from each other in the fact that Group 2 is enriched in LREE and depleted in Cr and Nb relative to Group 1 Kimberlites. The former is also H_2O rich, enriched in SiO_2, K_2O, Pb, Rb, and Ba (Sen, 2014).

References

Ablay, G.J., Carroll, M.R., Palmer, M.R., Marti, J., Sparks, R.S.J., 1998. Basanite−phonolite lineages of the Teide−Pico Viejo volcanic complex, Tenerife, Canary Islands. J. Petrol. 39 (5), 905−936.

Aliyari, F., Rastad, E., Mohajjel, M., Arehart, G.B., 2009. Geology and geochemistry of D−O−C isotope systematics of the Qolqoleh gold deposit, Northwestern Iran: implications for ore genesis. Ore Geol. Rev. 36 (4), 306−314.

Arribas, A., Mizuta, T., 2018. Potential for porphyry copper deposits in Northern Tohoku. Resource Geology, John Wiley & Sons. 68 (2), 144−163.

Bailey, R.A., Clark, H.M., Ferris, J.P., Krause, S., Strong, R.L., 2002. The earth's crust. In: Beiley, Ronald A. (Ed.), Chemistry of the Environment, second edition pp. 443−482, Academic Press, 835p.

Barnes, H.L., 2015. Hydrothermal processes. Geochem. Perspect. 4 (1), 1−93.

Bateman, A.M., 1950. Economic Mineral Deposits, second ed. John Wiley and Sons Inc, New York and London.

Begg, G.C., Hronsky, J.M.A., Griffin, W.L., O'Reilly, S.Y., 2018. Global- to deposit-scale controls on orthomagmatic Ni-Cu (-PGE) and PGE reef ore formation. Processes and Ore Deposits of Ultramafic-Mafic Magmas Through Space and Time. Elsevier, 1−46 pp.

Berning, J., Cooke, R., Heimstra, S.A., Hoffman, U., 1976. The Rössing Uranium Deposit, South West Africa. Econ. Geol. 71, 351−368.

Bertelli, M., Baker, T., Cleverley, J.S., Ulrich, T., 2009. Geochemical modelling of a Zn−Pb skarn: constraints from LA−ICP−MS analysis of fluid inclusions. J. Geochem. Explor. 102, 13−26.

Bodnar, R.J., Lecumberri-Sanchez, P., Moncada, D., Steele-MacInnis, M., 2014. 13.5-Fluid inclusions in hydrothermal ore deposits. In: Turekian, H.D.H.K. (Ed.), Treatise on Geochemistry, second ed Elsevier, Oxford, 119−142 pp.

Brugger, J., Liu, W., Etschmann, B., Mei, Y., Sherman, D.M., Testemale, D., 2016. A review of the coordination chemistry of hydrothermal systems, or do coordination changes make ore deposits? Chem. Geol. 447, 219−253. Available from: https://doi.org/10.1016/j.chemgeo.2016.10.021.

Casa, G.D., Manni, A., Saviano, G., Violo, G., 2003. Gold occurrence in Central Italy—the Ponte San Pietro mineralization. Ore Geol. Rev. 23, 99−105. Available from: https://doi.org/10.1016/S0169-1368(03)00017-9.

Černý, P., Ercit, T.S., Vanstone, P.J., 1996. Petrology and mineralization of the Tanco rare element pegmatite, southeastern Manitoba. Geological Association of Canada—Mineralogical Association of Canada, Joint Annual Meeting, Winnipeg 1996, Field Trip Guidebook A3, 63 pp.

Chivers, T., 1974. Ubiquitous trisulfur radical ion S^{-3}. Nature 252, 32–33.

Chou, I.M., 1978. Calibration of oxygen buffers at elevated P and T using the hydrogen fugacity sensor. Am. Min. 63, 690–703.

Cline, J.S., Hofstra, A.H., Muntean, J.L., Tosdal, R.M., Hickey, K., 2005. Carlin-type gold deposits in Nevada: critical geological characteristics and viable models. Economic Geology 100th Anniversary Volume. pp. 451–484.

Cooke, D.R., Simmons, S.F., 2000. Characteristics and genesis of epithermal gold deposits. Rev. Econ. Geol. 13, 221–244.

Corral, I., Cardellach, E., Corbella, M., Canals, À., Griera, A., Gómez-Gras, D., et al., 2017. Origin and evolution of mineralizing fluids and exploration of the Cerro Quema Au-Cu deposit (Azuero Peninsula, Panama) from a fluid inclusion and stable isotope perspective. Ore Geol. Rev. 80, 947–960.

Cox, D.P., Singer, D., 1986. Mineral Deposit Models. US Geological Survey Bulletin, Reston, VA.

Craig, J.R., Vaughan, D.J., 1981. Ore Microscopy and Ore Petrography. Wiley, New York.

Dai, J., Mao, J., Zhao, C., 2009. New U–Pb and Re–Os age data and the geodynamic setting of the Xiaojiayingzi Mo (Fe) deposit, western Liaoning province, Northeastern China New U–Pb and Re–Os age data and the geodynamic setting of the Xiaojiayingzi Mo (Fe) deposit, western Liaoning province, Northeastern China. Ore Geol. Rev. 35 (2), 235–244.

Dill, H.G., 2015. Pegmatites and aplites: their genetic and applied ore geology. Ore Geol. Rev. 69, 417–561. Available from: https://doi.org/10.1016/j.oregeorev.2015.02.022.

Einaudi, M., 2000. Mineral resources: assets and liabilities. In: Ernst, W.G. (Ed.), Earth Systems: Processes and Issues. Cambridge University Press, pp. 346–372.

Evans, A.M., 1993. Ore Geology and Industrial Minerals – An Introduction. Blackwell Scientific Publication, Oxford.

Evans, A.M., Moon, C.J., 2006. In: Moon, et al., (Eds.), Mineral Deposit Geology and Models, 2006. Blackwell, New York, 33–51 pp.

Evans, K.A., Reddy, S.M., Tomkins, A.G., Crossley, R.J., Frost, B.R., 2017. Effects of geodynamic setting on the redox state of fluids released by subducted mantle lithosphere. Lithos 278–281, 26–42.

Fiorentini, M.L., LaFlamme, C., Denyszyn, S., Mole, D., Maas, R., Locmelis, M., et al., 2018. Post-collisional alkaline magmatism as gateway for metal and sulfur enrichment of the continental lower crust. Geochimica et Cosmochimica Acta 223, 175–197.

Frost, B.R., Frost, C.D., 2014. Essentials of Igneous and Metamorphic Petrology. Cambridge University Press, New York.

Frost, B.R., Lindsley, D.H., Andersen, D.J., 1988. Fe–Ti oxide-silicate equilibrium: assemblages with fayalitic olivine. Am. Min. 73, 727–740.

Gaffney, J.S., Marley, N.A., 2018. Periodic table. General Chemistry for Engineers 623. Available from: https://doi.org/10.1016/b978-0-12-810425-5.09983-5.

Gammons, C.H., Williams-Jones, A.E., 1997. Chemical mobility of gold in the porphyry-epithermal environment. Econ. Geol. 92, 45–59.

González-Álvarez, I., Boni, M., Anand, R.R., 2016. Mineral exploration in regolith-dominated terrains: global considerations and challenges. Ore Geol. Rev. 73, 375–379.

Grand, S.P., 2002. Mantle shear-wave tomography and the fate of subducted slabs. Phil. Trans. R. Soc. Lon. (A3260), 2475–2491.

Groves, D.I., Vielreicher, R.M., Goldfarb, R.J., Condie, K.C., 2005. Controls on the heterogeneous distribution of mineral deposits through time. Geol. Soc. Lond. Spec. Publ. 248, 71–101.

Groves, D.I., Bierlein, F.P., Meinert, L.D., Hitzman, M.W., 2010. Iron-oxide copper gold (IOCG) deposits through Earth history: implications for origin, lithospheric setting, and distinction from other epigenetic iron oxide deposits. Econ. Geol. 105, 641–654.

Guilbert, J.M., Park, C.F., 1986. The Geology of Ore Deposits. W.H. Freeman and Co, New York, 985 pp.

Heinrich, C.A., Candela, P.A., 2014. Fluids and ore formation in the Earth's crust. In: Treatise on Geochemistry, pp. 1–28.

Holland, H.D., 2005. Sedimentary mineral deposits and the evolution of Earth's near-surface environments. Econ. Geol. 100, 1489–1509.

Hu, Z., Gao, S., 2008. Upper crustal abundances of trace elements: a revision and update. Chem. Geol. 253 (3–4), 205–221. Available from: https://doi.org/10.1016/j.chemgeo.2008.05.010.

Kazemi, K., Kananian, A., Xiao, Y., Sarjoughian, F., 2018. Petrogenesis of middle-Eocene granitoids and their Mafic microgranular enclaves in central Urmia-Dokhtar magmatic arc (Iran): evidence for interaction between felsic and mafic magmas. Geosci. Front. 10 (2), 705–723. Available from: https://doi.org/10.1016/j.gsf.2018.04.006.

Kesler, S.E., 1994. Mineral Resources, Economics and the Environment. McMillan, New York.

Kosman, C.W., Kopylova, M.G., Stern, R.A., Hagadorn, J.W., Hurlbut, J.F., 2016. Cretaceous mantle of the Congo craton: evidence from mineral and fluid inclusions in Kasai alluvial diamonds. Lithos 265, 42–56. Available from: https://doi.org/10.1016/j.lithos.2016.07.004.

Kotzer, T.G., Kyser, T.K., 1995. Petrogenesis of the proterozoic Athabasca Basin, Northern Saskatchewan, Canada, and its relation to diagenesis, hydrothermal uranium mineralization and paleohydrogeology. Chem. Geol. 120, 45–89.

Kress, V.C., Carmichael, I.S.E., 1991. The compressibility of silicate liquids containing Fe_2O_3 and the effect of composition, temperature, oxygen fugacity and pressure on their redox states. Contrib. Miner. Petrol. 108, 82–92.

Kretschmar, U., McBride, D., 2016. Understanding hydrothermal Systems. In: Kretschmar, Ulrich, McBride, Derek (Eds.), The Metallogeny of Lode Gold Deposits, pp. 151–198. First Edition Elsevier, 345p.

Kyser, K., 2016. Exploration for uranium. In: Hore Lacy, Ian (Ed.), Uranium for Nuclear Power, Resources Mining and transformation to fuel, pp. 53–76, First Edition Elsevier, 488p.

Laznicka, P., 2014. Giant metallic deposits—a century of progress. Ore Geol. Rev. 62, 259–314. Available from: https://doi.org/10.1016/j.oregeorev.2014.03.002.

Leach, D.L., Sangster, D.L., Kelley, K.D., Ross, R.L., Garven, G., Allen, C.R., 2005. Sediment-hosted Pb-Zn deposits: a global perspective. In: Hedenquist, J.W., Thompson, J.F.H., Goldfarb, R.J., Richards, J.P. (Eds.), Economic Geology 100th Anniversary, (1905–2005), pp. 5–24, Society of Economic Geologists, 1133p

Legros, H., Richard, A., Tarantola, A., Kouzmanov, K., Mercadier, J., Vennemann, T., et al., 2019. Multiple fluids involved in granite-related W-Sn deposits from the world-class Jiangxi province (China). Chem. Geol. 508, 92–115.

Liao, M., Tao, Y., Song, X., Li, Y., Xiong, F., 2016. Study of oxygen fugacity during magma evolution and ore genesis in the Hongge mafic–ultramafic intrusion, the Panxi region, SW China. Acta Geochim. 35 (1), 25–42.

Lindgren, W., 1922. A suggestion for the terminology of certain mineral deposits. Econ. Geol. 17 (4), 292–294.

Lindgren, W., 1933. Mineral Deposits, fourth ed McGraw-Hill, 930 pp.

Lindsley, D.H., 1991. Experimental studies of oxide minerals. Rev. Min. Geochem. 25, 69–106.

Macheyeki, A.S., 2011. Application of lithogeochemistry to exploration for Ni-Cu sulfide deposits in the Kabanga Belt, NW Tanzania. J. Afr. Earth Sci. 61, 62–81.
Maier, W.D., Groves, D.I., 2011. Temporal and spatial controls on the formation of magmatic PGE and Ni-Cu deposits. Mineralium Deposita 46, 841–858.
Mason-Apps, A.D., 1998. The petrology and geochemistry of the lower pyroxenite succession of the Great Dyke in the Mutorashanga area. Thesis submitted in partial fulfillment of the requirements for the Degree of Master of Science (Economic Geology) in the Department of Geology, Rhodes University, Grahamstown.
Meyer, C., 1981. Ore-forming processes in geologic history. In: Economic Geology, 75th Anniversary, pp. 6–41, The Economic Geology Publishing House, 960p.
Misra, K.C., 2000. Understanding Mineral Deposits. Kluwer Academic Publishers, p. 845.
Moon, C.J., 2016. In: Moon, et al., (Eds.), Exploration Geochemistry, 2006. Blackwell, New York, 156-198 pp.
Moon, C.J., Whateley, M.K.G., Evans, A.M., 2006. Introduction to Mineral Exploration, second ed Blackwell Publishing, New York.
Mungall, J.E., 2014. Geochemistry of magmatic ore deposits. In: Turikian, K.K., Holland, H.D. (Eds.), Treatise on Geochemistry, pp. 195–2181, Elsevier, 9144p.
Naldrett, A.J., 1997. Key factors in the genesis of Noril'sk, Sudbury, Jinchuan, Voisey's bay and other world-class Ni-Cu-PGE deposits: implications for exploration. Austr. J. Earth Sci. 44 (3), 283–315.
Naldrett, A.J., 2004. Magmatic Sulfide Deposits: Geology, Geochemistry and Exploration. Springer, New York, 730 pp.
Naldrett, A.J., 2010. From the mantle to the bank: the life of a Ni–Cu–(PGE) sulfide deposit. South Afr. J. Geol. 113, 1–32.
Niggli, P., 1929. In: Boydell, H.C. (Ed.), Ore Deposits of Magmatic Origin: Their Genesis and Natural Classification. Thomas Murby & Co, London, 93 pp.
O'Brien, H., 2015. Introduction to carbonatite deposits of Finland. Min. Depos. Finl. 291–303. Available from: https://doi.org/10.1016/b978-0-12-410438-9.00011-x.
Partington, G.A., 1990. Environment and structural controls on the intrusion of the giant rare metal Greenbushes pegmatite. West. Austr. Econ. Geol. 85, 437–456.
Peck, D.C., Huminicki, M.A.E., 2016. Value of mineral deposits associated with mafic and ultramafic magmatism: implications for exploration strategies. Ore Geol. Rev. 72, 269–298. Available from: https://doi.org/10.1016/j.oregeorev.2015.06.004.
Petrov, S.V., 2004. Economic deposits associated with the alkaline and ultrabasic complexes of the Kola Peninsula. In: Wall, V., Zaitsev, A.N. (Eds.), Phoscorites and Carbonatites from Mantle to Mine: the Key Example of the Kola Alkaline Province. Mineralogical Society, London, pp. 469–490.
Phillips, G.N., Evans, K.A., 2004. Role of CO_2 in the formation of gold deposits. Nature 429, 860–863.
Pokrovski, G.S., Dubessy, J., 2015. Stability and abundance of the trisulfur radical ion $S3^-$ in hydrothermal fluids. Earth Planet Sci. Lett. 411, 298–309.
Pun, A., Papike, J.J., Layne, G.D., 1997. Subsolidus REE partitioning between pyroxene and plagioclase in cumulate eucrites: an ion microprobe investigation. Geochimica et Cosmochimica Acta 61 (23), 5089–5097. Available from: https://doi.org/10.1016/s0016-7037(97)00295-0.
Richard, A., Cauzid, J., Cathelineau, M., Boiron, M.C., Mercadier, J., Cuney, M., 2013. Synchrotron XRF and XANES investigation of uranium speciation and element distribution in fluid inclusions from unconformity-related uranium deposits. Geofluids 13, 101–111.
Richards, J.P., 2011. Magmatic to hydrothermal metal fluxes in convergent and collided margins. Ore Geol. Rev. 40, 1–26.
Ridley, J., 2013. Ore Deposit Geology. Cambridge University Press, 409 pp.

Robb, L., 2005. Introduction to Ore-Forming Processes. Blackwell Sciences Ltd, Hoboken, NJ, 376 pp.
Rollinson, H.R., 1993. Using Geochemical Data: Longman Geochemistry Series, first ed. Routledge, 384 pp.
Rollinson, H., 2012. Geochemical constraints on the composition of Archaean lower continental crust: partial melting in the Lewisian granulites. Earth Planet. Sci. Lett. 351–352, 1–12. Available from: https://doi.org/10.1016/j.epsl.2012.07.018.
Rudnick, R.L., Gao, S., 2003. Composition of the continental crust. In: Rudnick RL (Ed.) Treatise on Geochemistry. The Crust (3), 1–64.
Sangster, D.F., 1980. Plate tectonics and mineral deposits: a view from two perspectives. Geosci. Canada 6 (4), 185–188.
Schneider H.J., 1964. Facies differentiation and controlling factors for depositional lead-zinc concentration in the Ladinian geosyncline of Eastern Europe. In: G.C. Amstutz (Ed.). Sedimentology and Ore Genesis, pp. 29–45.
Seedorff, E., Dilles, J., Proffett Jr., J.M., Einaudi, M.T., Zurcher, L., Stavast, W.J.A., et al., 2005. Porphyry deposits: characteristics and origin of hypogene features. In: Economic Geology 100th Anniversary (1905–2005). Society of Economic Geologists, pp. 251–298.
Sen, G., 2014. Petrology: Principle and Practice. Springer, Heidelberg-Berlin.
Seward, T.M., Barnes, H.L., 1997. Metal transport by hydrothermal ore fluids. In: Barnes, H. L. (Ed.), Geochemistry of Hydrothermal Ore Deposits. John Wiley & Sons, pp. 435–486.
Seward, T.M., Williams-Jones, A.E., Migdisov, A.A., 2014. The chemistry of metal transport and deposition by ore-forming hydrothermal fluids. Treat. Geochem. 29–57. Available from: https://doi.org/10.1016/b978-0-08-095975-7.01102-5.
Shvarov, Y., Bastrakov, E.H.Ch, 1999. A Software Package for Geochemical Equilibrium Modelling. User's Guide (Record 1999/25, Australian Geological Survey Organization).
Stanton, R.L., 1972. Ore Petrology. McGraw-Hill Book Co, London and New York, 713 pp.
Steudel, R., Steudel, Y., 2013. Polysulfide chemistry in sodium–sulfur batteries and related systems—a computational study by G3X(PM2) and PCM calculations. Chem. Eur. J. 19, 3162–3176.
Stowe, C.W., 1994. Composition and tectonic settings of chromite deposits through time. Econ. Geol. Bull. Soc. Econ. Geol. 89, 528–546.
Sun, W., Xing, M.L., Yong, Y.X., WeiMing, F., Xing, D., Ying, L.H., 2010. Ridge subduction and porphyry copper-gold mineralization: an overview. Sci. China, Earth Sci. 53 (4), 475–484.
Sun, W., Huang, R., Li, H., Hu, Y., Zhang, C., Sun, S., et al., 2015. Porphyry deposits and oxidized magmas: a review. Ore Geol. Rev. 65, 97–131.
Taylor, H.P., 1997. Oxygen and hydrogen isotope relationships in hydrothermal mineral deposits. In: Barnes, H.L. (Ed.), Geochemistry of hydrothermal ore deposits, third ed John Wiley & Sons, New York, pp. 229–302.
Trail, D., Bindeman, I.N., Watson, E.B., Schmitt, A.K., 2009. Experimental calibration of oxygen isotope fractionation between quartz and zircon. Geochimica et Cosmochimica Acta 73 (23), 7110–7126.
Trail, D., Watson, E.B., Tailby, N.D., 2012. Ce and Eu anomalies in zircon as proxies for the oxidation state of magmas. Geochim. Cosmochim. Acta 97, 70–87.
Tucker, R.F., Viljoen, R.P., Viljoen, M.J., 2016. A review of the Witwatersrand Basin: the world's greatest goldfield. Episodes 39 (2), 105.
Vigneresse, J.L., 2019. Addressing ore formation and exploration. Geosci. Front. 10 (4), 1613–1622.
Viter, P., Léo, A.H., Henrique, R.L., Carlos, K.J., Evaldo, S., Vinícius, R.M., et al., 2013. Geology, ore characterization and fluid inclusions study of gold deposits from the Campestre Formation, Southernmost Brazil. c02. Recursos Minerales. Montesinos de Almeida, Delia del Pilar Brasil–UFPel; UFRGS; UNIPAMPA.

Westphal, G., Kristen, G., Wegener, W., Ambatiello, P., Geyer, H., Epron, B., et al., 2010. Sodium Chloride. Wiley-VCH Verlag GmbH & Co, Weinheim.
White, W.M., Patchett, J., 1984. HfNdSr isotopes and incompatible element abundances in island arcs: implications for magma origins and crust-mantle evolution. Earth Planet Sci. Lett. 67 (2), 167–185. Available from: https://doi.org/10.1016/0012-821x(84)90112-2.
Williams, P.J., Barton, M.D., Johnson, D.A., Fontbote, L., De Haller, A., Mark, G., et al., 2005. Iron oxide copper gold deposits: geology, space-time distribution and possible modes of origin. Economic Geology 100th Anniversary Volume, 371–405.
Xiong, X., Zhu, L., Zhang, G., Li, N., Yuan, H., Ding, L., et al., 2018. Fluid inclusion geochemistry and magmatic oxygen fugacity of the Wenquan Triassic molybdenum deposit in the Western Qinling Orogen, China. Ore Geol. Rev. 99, 244–263.
Yang, Q.-Y., Santosh, M., 2015. Early cretaceous magma flare-up and its implications on gold mineralization in the Jiaodong Peninsula, China. Ore Geol. Rev. 65, 626–642. Available from: https://doi.org/10.1016/j.oregeorev.2014.01.004.
Zhou, T., Zeng, Q., Chu, S., Zhou, L., Yang, Y., 2018. Magmatic oxygen fugacities of porphyry Mo deposits in the East Xing'an-Mongolian Orogenic Belt (NE China) with metallogenic implications. J. Asian Earth Sci . Available from: https://doi.org/10.1016/j.jseaes.2018.04.004.
Zhu, Y., An, F., Tan, J., 2011. Geochemistry of hydrothermal gold deposits: a review. Geosci. Front. 2 (3), 367–374.

Further reading

Allen, P.A., 1997. Earth Surface Processes. Blackwell Science, Oxford, 404 pp.
Bianconi, F., Borshoff, J., 1984. Surficial Uranium occurrences in United Republic of Tanzania. Surficial Uranium Deposit. IAEA, Vienna, pp. 231–235.
Boniface, N., 2017. Crystal chemistry of pyrochlore from the Mesozoic Panda Hill carbonatite deposit, western Tanzania. J. Afr. Earth Sci. 126, 33–44.
Borg, G., Krogh, T., 1999. Isotopic age data of single zircons from the Archaean Sukumaland Greenstone Belt, Tanzania. J. Afr. Earth Sci. 29, 301–312.
Bowell, R.J., Barnes, A., Grogan, J., Dey, M., 2009. Geochemical Control on Uranium Precipitation in Calcrete Palae Channel Deposits of Namibia. SRK Publications, pp. 1–4.
Carlisle, D., 1984. Surficial Uranium Occurrences in Relation to Climate and Physical Setting. Surficial Uranium Deposit. IAEA, Vienna, pp. 25–35.
Chamberlain, C.M., Tosdal, R.M., 2007. U–Pb geochronology of the Lake Victoria Greenstone Terrane, Tanzania. Mineral Deposit Research Unit, The University of British Columbia. Unpublished Geita Gold Mine internal report, pp. 81.
Craig, J.R. and Vaughan, D.J., 1986. Paragenetic studies of growth-banded sphalerites in Mississippi Valley-type zinc deposits of the Appalachians. In: Augustithes, S.S. (Ed.), Mineral Paragenesis, pp. 133–158.
de Klerk, S.-L., 2001. Gold deposits in the SADC region, mineral resources survey programme No. 4, SADC Mining Sector Coordinating Unit, Council for Geoscience, 126 pp.
De Pierre, M., Coron, N., Dambier, G., Leblanc, J., Moalic, J.-P., 2003. Experimental detection of α-particles from the radioactive decay of natural bismuth. Nature 422 (6934), 876–878.
Evans, D.M., Boad, I., Byemelwa, L., Gilligan, J., Kabete, J., Marcet, P., 2000. Kabanga magmatic nickel sulfide deposits, Tanzania: morphology and geochemistry of associated intrusions. J. Afr. Earth Sci. 30 (3), 651–674.

Evans, D.M., Hunt, J.P.P.M., Simmonds, J.R., 2016. An overview of Nickel mineralization in Africa with emphasis on the Mesoproterozoic East African Nickel Belt (EANB). In: Wilson and Viljoen (2016) on Special Issue for the 35 IGC, Cape Town, South Africa.

Feneyrol, J., Giuliani, G., Ohnenstetter, D., Fallick, A.E., Martelat, J.M., Monie, P., et al., 2017. Age and origin of the tsavorite and tanzanite mineralizing fluids in the neproterozoic Mozambique Metamorphic belt. Can. Min. 55, 763–786.

Geosurvey International GMbH, 1981. Synoptic map showing the gold potential of the Archean Greenstone Belts, scale 1:500,000.

Geosurvey International GMbH, 1982. An economic appraisal of the mineral potential of the United Republic of Tanzania, Report printed for the Ministry of Energy and Minerals, Tanzania.

Giuliani, G., Ohnenstetter, D., Palhol, F., Feneyrol, J., Boutroy, E., De Boissezon, H., et al., 2008. Karelianite and vanadian phlogopite from the Merelani Hills gem zoisite deposits, Tanzania. Can. Min. 46, 1183–1194.

Haggerty, S.E., 1999. A diamond trilogy: super plumes, supercontinents and supernovae. Science 285, 851–860.

Haldar, S.K., 2013. Mineral Exploration: Principles and Applications. Elsevier, China.

Haldar, S.K., 2017. Platinum-Nickel-Chromium Deposits: Geology, Exploration and Reserve Base. Elsevier, 322p.

Harland, W.B., Armstrong, R.L., Cox, A.V., Craig, L.E., Smith, A.G., Smith, D.G., 1990. A Geological Time Scale, 1989. Cambridge University Press, 263 pp.

Harris, F.J., 1961a. Summary of the Geology of Tanganyika. Part IV, Economic Geology Memoir No. 1. Dodoma Government Printer.

Harris, J.F., 1961b. Summary of the Geology of Tanzania, Economic Geology. Tanzania Geological Survey, Dodoma, Tanzania.

Harris, F.J., 1969. Kaolin deposit of Tanzania, international Geological Congress Report of the twenty third session, Czechslovakia, 1969, Proceeding of the Symposium 1. Kaolin deposit of the world, B-Oversea Contributions, 75–78.

Heirtzler, J.R., Dickson, G.O., Herron, E.M., Pitman, W.C., Le Pichon, X., 1968. Marine magnetic anomalies, geomagnetic field reversals and motions of the ocean floor and continents. J. Geophys. Res. 73, 2119–2136.

ICS 2000 edition of the International Stratigraphic Chart published and sanctioned by the ICS and IUGS. <http://www.angelfire.com/sc3/farooqs/notes/b3-3-1.htm>.

Jansson, N.F., Zetterqvist, A., Allen, R.L., Billström, K., Malmström, L., 2017. Genesis of the Zinkgruvan stratiform Zn-Pb-Ag deposit and associated dolomite-hosted Cu ore, Bergslagen, Sweden. Ore Geol. Rev. 82, 285–308.

Kabete, J.M., Groves, D.I., McNaughton, N.J., Mruma, A.H., 2012. A new tectonic and temporal framework for the Tanzanian Shield: implications for gold metallogeny and undiscovered endowment. Ore Geol. Rev. 48, 88–124.

Kazimoto, E.O., Schenk, V. and Appel, P., 2015. The age of Au–Cu–Pb-bearing veins in the poly-orogenic Ubendian Belt (Tanzania): U–Th–total Pb dating of hydrothermally altered monazite, In: Contributions to Mineralogy and Petrology *Petrology*. Springer-Verlag Berlin Heidelberg 169, 1088.

Keller, W.D., 1978. Classification of kaolins exemplified by their textures in scan electron micrographs. Clays Min. 26, 1–20.

Lawley, C.J.M., Selby, D., Condon, D.J., Horstwood, M., Millar, I., Crowley, Q., et al., 2014. Lithogeochemistry, geochronology and geochronology and geodynamic setting of the Lupa Terrane, Tanzania: implications for the Archean Tanzania Craton. Precambrian Res. 231, 174–193.

Li, Y., Audétat, A., 2013. Gold solubility and partitioning between sulfide liquid, monosulfide solid solution and hydrous mantle melts: implications for the formation of Au-rich

magmas and crust–mantle differentiation. Geochimica et Cosmochimica Acta 118, 247–262.
Li, Z.X., Bogdanova, S.V., Collins, A.S., Davidson, A., Waele, B. De, Ernst, R.E., et al., 2008. Assembly, configuration, and break-up history of Rodinia: a synthesis. Precambrian Res. 160, 179–210.
Maier, W.D., Barnes, S.J., de Waal, S.A., 1998. Exploration for magmatic Ni-Cu-PGE sulphide deposits: a review of recent advances in the use of geochemical tools, and their application to some South African Ores. South Afr. J. Geol. 101 (3), 237–253.
Malisa, E., Mhuhongo, S., 1990. Tectonic setting of gemstone mineralization in the Proterozoic metamorphic terrane of the Mozambique Belt in Tanzania. Precambrian Res. 46, 167–176.
McKinlay, A.C.M., 1965. The Coalfields and Coal Resources of Tanzania. Tanzania Geological Survey, Dodoma, Tanzania, Bulletin No. 38.
McQueen, K.G., 1987. Deformation and remobilization in some Western Australian nickel ores. Ore Geol. Rev. 2 (1–3), 269–286.
McQueen, K.G., 2006. Geochemical fractionation in the regolith of western New South Wales. Geochimica et Cosmochimica Acta 70 (18), A415.
MEM, 2005: TANZANIA: Opportunities for Mineral Resources Development, Ministry of Energy and Minerals, Dares-Salaam, Tanzania.
Mtelela, C., 2016. Sedimentology and Stratigraphy of the Late Cenozoic Lake Beds Succession, Rukwa Rift Basin, Tanzania: Implications for Hydrocarbon Prospectivity (PhD thesis). James Cook University.
Nance, R.D., Worsley, T.R., Moody, J.B., 1986. Post-Archean biogeochemical cycles and long-term episodicity in tectonic processes. Geology 14, 514–518.
Parnell, J., Ye, L., Chen, C., 1990. Sediment-hosted mineral deposits. Special Publication, 11, International Association of Sedimentologists. Blackwell Scientific Publications, Oxford, 227 pp.
Pearson, R.G., 1963. Hard and soft acids and bases. J. Am. Chem. Soc. 85, 3533–3539.
Reeves, C.V., de Wit, M.J., Sahu, B.K., 2004. Tight reassembly of Gondwana exposes Phanerozoic shears in Africa as global tectonic players. Gondwana Res. 7 (I), 7–19.
Richard, A., 2017. Radiolytic (H_2, O_2) and other trace gases (CO_2, CH4, C_2H_6, N_2) in fluid inclusions from unconformity-related U deposits. 15th Water-Rock Interaction International Symposium, WRI-15. Procedia Earth and Planetary Science 17, 273–276.
Richard, A., Banks, D.A., Hendriksson, N., Lahaye, Y., 2018. Lithium isotopes in fluid inclusions as tracers of crustal fluids: an exploratory study. J. Geochem. Explor. 184, 158–166.
Richards, J.P., 2013. Giant ore deposits formed by optimal alignments and combinations of geological processes. Nat. Geosci. 6, 911–916.
Roedder, E., 1976. Fluid-inclusion evidence on the genesis of ores in sedimentary and volcanic rocks. In: Wolf, K.H. (Ed.), Handbook of Stratabound and Stratiform Ore Deposits., 2. Elsevier, Amsterdam, pp. 67–110.
Roedder, E., 1979. Fluid inclusions as samples of ore Fluids. In: Barnes, H.L. (Ed.), Geochemistry of Hydrothermal Ore Deposits, second ed. Wiley-Interscience, New York, 614-737 pp.
Sango, P.M., 1988. Structural and Lithological controls of gold mineralization in the Lupa goldfields, Tanzania. In: Ho, S.E., Groves, D.I. (Eds.), Recent Advances in understanding Precambrian Gold Deposits, 12. Geology Department and University Extension, The University of Western Australia, Publication, pp. 99–109.
Sanislav, I.V., Wormald, R.J., Dirks, P.H.G.M., Blenkinsop, T.G., Salamba, L., Joseph, D., 2014a. Zircon U-Pb ages and Lu-Hf isotope systematic from late-tectonic granites, Geita greenstone belt: implications for crustal growth of the Tanzania craton. Precambrian Res. 242, 187–204.

Sanislav, I.V., Dirks, P.H.G.M., Cook, Y.A., Blenkinsop, T.G., Kolling, S.L., 2014b. A Giant Gold System, Geita Greenstone Belt, Tanzania. ACTA Geologica Sinica (English Edition) 88 (Suppl), 2.

Sanislav, I.V., Kolling, S.L., Brayshaw, M., Cook, Y.A., Dirks, P.H.G.M., Blenkinsop, T.G., et al., 2015. The geology of the giant Nyankanga gold deposit, Geita Greenstone Belt, Tanzania. Ore Geol. Rev. 69, 1–16.

Sanislav, I.V., Brayshaw, M., Kolling, S.L., Dirks, P.H.G.M., Cook, Y.A., Blenkinsop, T.G., 2016. The structural history and mineralization controls of the world-class Geita Hill gold deposit, Geita Greenstone Belt, Tanzania. Miner Deposita 52 (2), 292–315. Available from: https://doi.org/10.1007/s00126-016-0660.

Schwaighofer, B., Muller, H.W., 1987. Mineralogy and genesis of the Pugu Hill Kaolin. Clay Min. 22, 401–409.

Selley, R.C., 1998. Elements of Petroleum Geology, second ed Academic Press, New York, 470 pp.

Smith, W., Sandwell, D., 1997. Measured and estimated seafloor topography (version 4.2). World Data Center A for Marine Geology and Geophysics Res. publ. RP-1, poster, 34″ x 53″.

Song, X., Wang, Y., Chen, L., 2011. Magmatic Ni-Cu-(PGE) deposits in magma plumbing systems: features, formation and exploration. Geosci. Front. 2 (3), 375–384.

Stein, M., Hofmann, A.W., 1994. Mantle plumes and episodic crustal growth. Nature 372, 63–67.

Stiefenhofer, Farrow, 2004. Geology of the Mwadui kimberlite, Shinyanga district, Tanzania. Lithos 76 (1), 139–160.

Sun, W., 2017. The initiation of plate subduction. Solid Earth Sci. 2 (4), 89–90. Available from: https://doi.org/10.1016/j.sesci.2017.10.001.

Switzer, G.S., 1974. Composition of green garnet from Tanzania and Kenya. Gems Gemol. 14, 296–297.

Tack, L., Wingate, M.T.D., De Waele, B., Meert, J., Belousova, E., Griffin, B., et al., 2010. The 1375 Ma "Kibaran event" in Central Africa: prominent emplacement of bimodal magmatism under extensional regime. Precambrian Res. 180, 63–84.

Thomas, R.J., Spencer, C., Bushi, A.M., Baglow, N., Boniface, N., Kock, G., et al., 2016. Geochronology of the central Tanzania Craton and its southern and eastern orogenic margins. Precambrian Res. 277, 47–67.

Torsvik, T.H., Smethurst, M.A., Meert, J.G., Van der Voo, R., McKerrow, W.S., Sturt, B.A., et al., 1996. Continental break-up and collision in the Neoproterozoic and Palaeozoic – a tale of Baltica and Laurentia. Earth-Sci. Rev. 40, 229–258.

White, W.M., 2013. Geochemistry, first ed Wiley-Blackwell, Oxford, 660 pp.

White, W.M., Klein, E.M., 2014. Composition of the oceanic Crust. Treat Geochem. 457–496. Available from: https://doi.org/10.1016/b978-0-08-095975-7.00315-6.

Windley, B.F., 1995. The Evolving Continents, third ed. John Wiley & Sons, New York, Brisbane, Toronto, Singapore, xvii + 526 pp. Chichester.

Xu, C., Wang, L., Song, W., Wu, M., 2010. Carbonatites in China: a review for genesis and mineralization. Geosci. Front. 1 (1), 105–114. Available from: https://doi.org/10.1016/j.gsf.2010.09.001.